JEM Journal of Experimental Medicine

ARTICLE

P2X7 receptor restrains pathogenic Tfh cell generation in systemic lupus erythematosus

Caterina E. Faliti[1,2], Roberta Gualtierotti[3,4], Elsa Rottoli[1,5], Maria Gerosa[3,4], Lisa Perruzza[1,2], Andrea Romagnani[1,2], Giovanni Pellegrini[6], Benedetta De Ponte Conti[1,5], Riccardo L. Rossi[7], Marco Idzko[8], Emilia M.C. Mazza[9], Silvio Bicciato[9], Elisabetta Traggiai[10], Pier Luigi Meroni[3,4,11], and Fabio Grassi[1,5,7]

Altered control of T follicular helper (Tfh) cells can lead to generation of autoantibodies and autoimmune manifestations. Signaling pathways that selectively limit pathogenic responses without affecting the protective function of Tfh cells are unknown. Here we show that the ATP-gated ionotropic P2X7 receptor restricts the expansion of aberrant Tfh cells and the generation of self-reactive antibodies in experimental murine lupus, but its activity is dispensable for the expansion of antigen-specific Tfh cells during vaccination. P2X7 stimulation promotes caspase-mediated pyroptosis of Tfh cells and controls the development of pathogenic ICOS$^+$ IFN-γ–secreting cells. Circulating Tfh cells from patients with systemic lupus erythematosus (SLE) but not primary antiphospholipid syndrome (PAPS), a nonlupus systemic autoimmune disease, were hyporesponsive to P2X7 stimulation and resistant to P2X7-mediated inhibition of cytokine-driven expansion. These data point to the P2X7 receptor as a checkpoint regulator of Tfh cells; thus, restoring P2X7 activity in SLE patients could selectively limit the progressive amplification of pathogenic autoantibodies, which deteriorate patients' conditions.

Introduction

T follicular helper (Tfh) cells are a specialized subset of effector CD4 T cells that play a crucial role in the generation of protective antibody responses against pathogens. However, dysfunctional Tfh cells can activate autoantibody-producing B cells that cause autoimmunity (Yu and Vinuesa, 2010; Craft, 2012; Crotty, 2014). Understanding the regulatory mechanisms that ensure the homeostatic control of Tfh cell activation can provide insight for manipulating T cell–dependent antibody responses in autoimmune conditions. The Tfh cell differentiation program is implemented by up-regulation of inducible T cell costimulator (ICOS) that induces the transcription factor Bcl6 (Nurieva et al., 2008; Choi et al., 2011). Bcl6 in turn promotes CXCR5 expression and migration of the developing Tfh cell to the B cell follicle (Choi et al., 2011; Pepper et al., 2011). The concomitant down-regulation of CCR7 and P-selectin glycoprotein ligand 1 (PSGL-1) allows the T cell to exit the T cell zone and colocalize with B cells. The ICOS–ICOSL interaction is important in mediating Tfh cell migration to the B cell follicle (Xu et al., 2013). Antigen presentation and ICOSL expression by B cells are instrumental to the expansion of Tfh cells, resulting in germinal center (GC) formation.

ATP is a ubiquitous extracellular messenger that can act also as a danger-associated molecular pattern; it activates purinergic receptors in the plasma membrane termed P2 receptors. The P2X7 receptor subtype is an ATP-gated nonselective cationic channel characterized by dual gating: whereas P2X7 stimulation with ATP in the hundred-micromolar range leads to opening of a cytolytic pore and cell death, receptor exposure to low concentrations of ATP (e.g., micromolar range) results in small-amplitude currents (Khadra et al., 2013). The *P2rx7* gene, encoding for P2X7, is widely expressed, with the highest levels in cells from nervous and immune systems. Tfh cells express high levels of P2X7 in the plasma membrane; in the Peyer's patches (PPs) of the small intestine, they are exposed to extracellular concentrations of ATP that promote cell death via P2X7. Consequently, Tfh cells with deletion of *P2rx7* show resistance to extracellular ATP (eATP)–induced pore opening and cell death. The improved helper activity

[1]Institute for Research in Biomedicine, Università della Svizzera Italiana, Bellinzona, Switzerland; [2]Graduate School for Cellular and Biomedical Sciences, University of Bern, Bern, Switzerland; [3]Department of Clinical Science and Community Health, University of Milan, Milan, Italy; [4]Lupus Clinic, IASST-Istituto Gaetano Pini, Milan, Italy; [5]Department of Medical Biotechnology and Translational Medicine, University of Milan, Milan, Italy; [6]Laboratory for Animal Model Pathology, Institute of Veterinary Pathology, Vetsuisse Faculty, University of Zurich, Zurich, Switzerland; [7]Istituto Nazionale Genetica Molecolare "Romeo ed Enrica Invernizzi," Milan, Italy; [8]Division of Pulmonology, Department of Medicine II, Medical University of Vienna, Vienna, Austria; [9]Department of Life Sciences, University of Modena and Reggio Emilia, Modena, Italy; [10]Novartis Institute for Biomedical Research, Basel, Switzerland; [11]Istituto Auxologico Italiano, Milan, Italy.

Correspondence to Fabio Grassi: fabio.grassi@irb.usi.ch; Pier Luigi Meroni: pierluigi.meroni@unimi.it.

of *P2rx7*$^{-/-}$ Tfh cells results in enhanced GC reaction, IgA secretion, and binding to commensals (Proietti et al., 2014).

It is not clear whether eATP might influence Tfh cells at inflammatory sites, where it is present at high concentrations (Wilhelm et al., 2010). We addressed this issue in chronic inflammation elicited by pristane injection that causes a lupus-like syndrome in mice (Satoh and Reeves, 1994; Reeves et al., 2009). We show that lack of P2X7 in Tfh cells significantly worsened the disease by enhancing the generation of autoantibodies. Notably, circulating Tfh cells from patients with SLE were almost insensitive to P2X7-mediated control. In contrast, Tfh cells from patients with primary antiphospholipid syndrome (PAPS) were inhibited by P2X7 stimulation, suggesting that impaired P2X7 activity selectively contributes to the immunopathogenesis of SLE.

Results

P2rx7 deletion exacerbates immunopathology in experimental murine lupus

Several key features of SLE can be induced in mice by a single i.p. injection of the hydrocarbon oil 2,6,10,14-tetramethylpentadecane (commonly known as "pristane"; Satoh and Reeves, 1994; Reeves et al., 2009), which provokes peritoneal inflammation, production of antinuclear antibodies (ANAs) and glomerulonephritis. *P2rx7*$^{-/-}$ mice treated with pristane showed more severe splenomegaly (Fig. 1 A). Pristane-induced lupus (PIL) is characterized by peritoneal lipogranulomas, ectopic lymphoid structures that sustain autoantibody production (Nacionales et al., 2009; Weinstein et al., 2013). We observed more widespread lipogranulomas and enhanced glomerular damage in *P2rx7*$^{-/-}$ compared with WT mice (Fig. 1 C). Consistent with these findings, proteinuria levels (Fig. 1 B) and IgG immunocomplexes as well as complement C3 deposits in the glomeruli (Fig. 1 D) were markedly increased in mice lacking P2X7. Overall, these results indicate that *P2rx7* deletion exacerbates pristane-induced immunopathology.

P2rx7 deletion leads to enhanced secretion of self-reactive antibodies and abnormal GC reaction

Administration of pristane results in hypergammaglobulinemia and production of ANAs, a hallmark of SLE (Satoh and Reeves, 1994; Reeves et al., 2009). The serum concentrations of IgG, particularly IgG_1 and IgG_{2B} subtypes, were significantly augmented in *P2rx7*$^{-/-}$ with respect to WT mice, whereas IgG_{2C}, IgM, and IgG_3 were comparable in the two groups of animals (Fig. 2 A). Indirect immunofluorescence assay with HEp-2 cells revealed predominant staining patterns classified as "dominant homogenous" and "mixed homogeneous/nucleolar" with sera from *P2rx7*$^{-/-}$ mice, suggesting robust generation of autoantibodies directed against nuclear components, whereas sera from WT mice preferentially showed cytoplasmic and mixed cytoplasmic/nucleolar patterns with minimal reactivity (8% of tested sera) to homogeneous/nuclear antigens (Fig. 2 B). Semiquantitative detection of IgG reactive to SLE-specific self-antigens showed significant increases of self-reactive IgG in sera from pristane-treated *P2rx7*$^{-/-}$ mice, which showed values more similar to those of autoimmune-prone Murphy Roths Large/Lymphoproliferative (MRL/*lpr*) than to WT mice (Fig. 2 C).

The generation of self-reactive antibodies might originate from dysregulated immune checkpoint function during B cell differentiation. Analysis of the splenic B cell compartment at 8 mo after pristane administration did not reveal differences in the distribution of follicular and marginal zone B cells between WT and *P2rx7*$^{-/-}$ mice (Fig. S1 A). Conversely, splenic plasma cells (Fig. 2 E) as well as IgG-secreting cells (Fig. 2 D) were more abundant in *P2rx7*$^{-/-}$ mice. Serum autoantibodies can be generated through both extrafollicular and GC-derived pathways, the latter likely promoting somatic hypermutation and IgG affinity maturation. The contribution of GC B cells to PIL immunopathogenesis has not been directly explored so far. Splenic PNA^{+}Fas^{+} GC B cells were unaltered in pristane-treated WT mice with respect to untreated animals at 8 mo after pristane administration. However, these cells were significantly increased in *P2rx7*$^{-/-}$ mice (Fig. 3 A), as were the number and size of GCs detected by immunofluorescence staining of spleen cryosections (Fig. 3 B). These experiments suggest that protracted GC reaction could be responsible for the enrichment of autoreactive IgG in *P2rx7*$^{-/-}$ mice.

P2rx7 deletion favors the generation of pathogenic Tfh and kidney-infiltrating T cells in PIL

Pristane administration induced a significant expansion of effector/memory CD4 cells in *P2rx7*$^{-/-}$ mice compared with WT mice (Fig. S1 B). Among effector T cells, Tfh cells are specialized to provide help to B cells and crucially contribute to GC regulation. Aberrant expansion of Tfh cells is a common feature of SLE as well as of several spontaneous and induced models of murine lupus. Indeed, flow cytometry and immunofluorescence confirmed the follicular localization (Fig. 3 B) and expansion of Tfh cells expressing ICOS and PD-1 (Fig. 3 C) in pristane-treated *P2rx7*$^{-/-}$ compared with WT mice. Down-regulation of CCR7 and high expression of PD-1 define the immunopathogenic Tfh cell phenotype in lupus-prone *sanroque* mice (He et al., 2013). Analogously, CCR7$^{lo/-}$PD-1^{hi} Tfh cells were significantly increased in the spleen of pristane-treated *P2rx7*$^{-/-}$ with respect to WT mice (Fig. 3 D). ICOS amplification results in spontaneous autoimmune manifestations in *sanroque* mice (Vinuesa et al., 2005) and increased IgG production as well as multiorgan inflammation in autoimmune-prone MRL/*lpr* mice (Odegard et al., 2008; Teichmann et al., 2015). ICOS-expressing CD4 cells promote nephritis in lupus-prone mice (Odegard et al., 2009) and were detected in renal biopsy of patients with lupus nephritis (Hutloff et al., 2004; Cohen et al., 2008). In *P2rx7*$^{-/-}$ mice, kidney-infiltrating ICOS^{+} CD4 cells were significantly increased following pristane administration (Fig. S2, A and B), likely contributing to the severe glomerular damage observed in these mutant mice.

Immunosuppressive T regulatory (T reg) cells limit the expansion of autoreactive cells and are considered as potential therapeutic tools in autoimmune conditions. Their defect might contribute to lupus pathogenesis, although a specific role in human SLE is debated (Ohl and Tenbrock, 2015). We did not detect differences in T reg cell representation in the spleen between pristane-injected WT and *P2rx7*$^{-/-}$ mice (Fig. S1 C). Moreover, we addressed whether T follicular regulatory (Tfr) cells, which represent specialized T reg cells controlling GC reaction (Chung

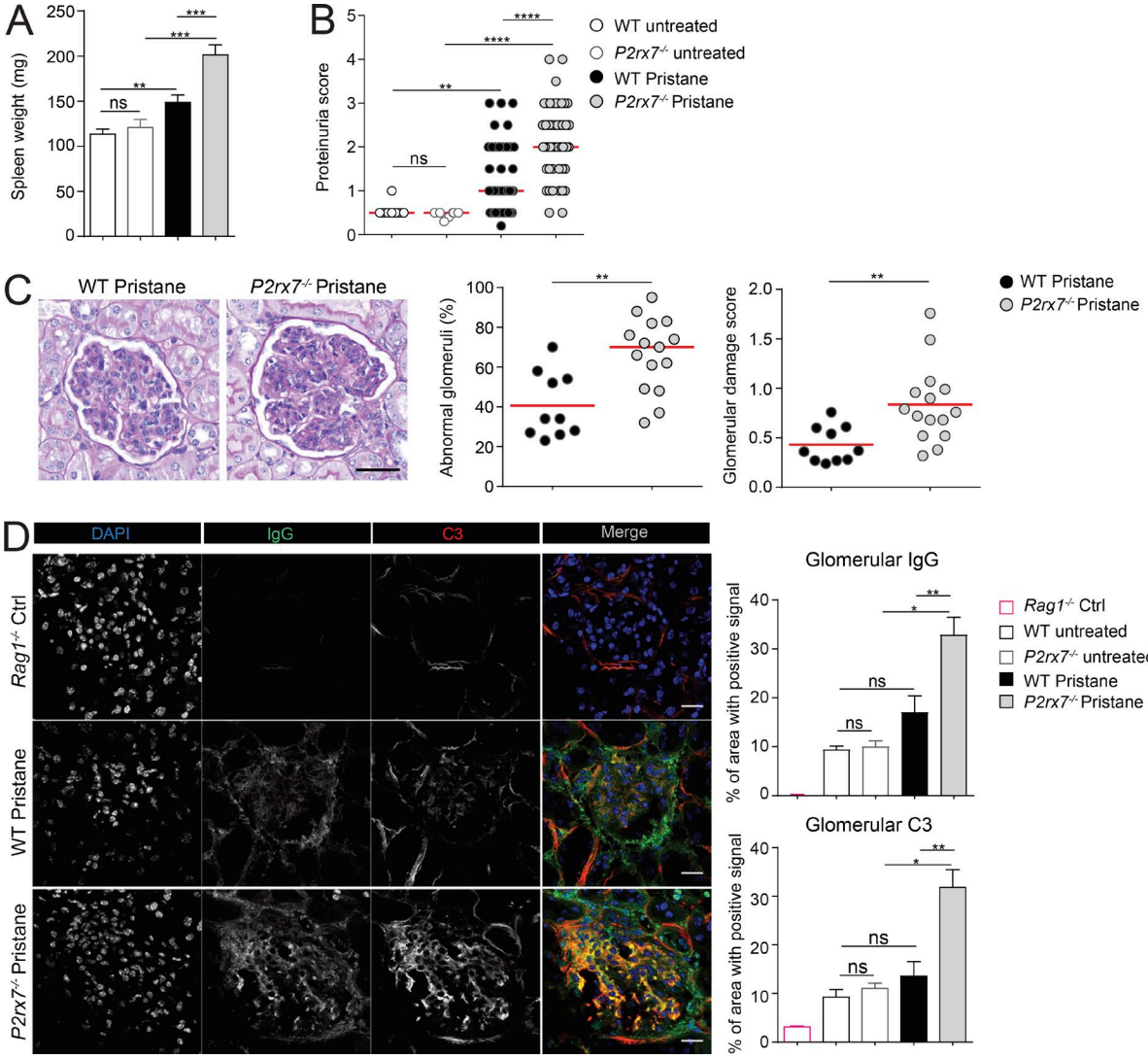

Figure 1. **Increased lupus nephritis severity in *P2rx7*$^{-/-}$ mice. (A)** Spleen weight of untreated WT (n = 7), *P2rx7*$^{-/-}$ (n = 6), pristane-treated WT (n = 19), and *P2rx7*$^{-/-}$ (n = 18) mice. **(B)** Proteinuria score of pristane-treated WT and *P2rx7*$^{-/-}$ mice. Each dot represents an individual mouse, and horizontal lines represent median values. WT untreated (n = 8), *P2rx7*$^{-/-}$ untreated (n = 8), WT pristane (n = 47), *P2rx7*$^{-/-}$ pristane (n = 53). **(C)** Representative pristane-induced glomerular injury in periodic-acid-Schiff–stained kidney sections (bar, 50 µm) with proportion of affected glomeruli (left graph) and glomerular injury score (right graph). WT pristane (n = 10), *P2rx7*$^{-/-}$ pristane (n = 15). **(D)** Confocal microscopy of kidneys stained for IgG (green) and complement C3 (red) to detect glomerular immune deposits. *Rag1*$^{-/-}$ mice were used as negative control for IgG staining (bars, 20 µm). Histograms show means ± SEM for glomerular IgG (top) and C3 depositions (bottom) of three independent experiments. *Rag1*$^{-/-}$ Ctrl (n = 2), WT untreated (n = 3), *P2rx7*$^{-/-}$ untreated (n = 3), WT pristane (n = 8), *P2rx7*$^{-/-}$ pristane (n = 10). All data are from mice at 33 wk after injection. Two-tailed Mann–Whitney U test. *, P < 0.05; **, P < 0.01; ***, P < 0.001; ****, P < 0.0001. ns, not significant.

et al., 2011; Linterman et al., 2011; Wollenberg et al., 2011), were affected in *P2rx7*$^{-/-}$ mice. However, we did not detect differences in Tfh/Tfr or GC B/Tfr cell ratios in the spleen of treated animals (Fig. S1 D), suggesting that *P2rx7*$^{-/-}$ Tfr cells efficiently expanded concomitantly to enhanced Tfh and GC B cells expansion. Therefore, it seems unlikely they might contribute to deregulated GC reaction in *P2rx7*$^{-/-}$ mice.

P2X7 activity limits the expansion of Tfh cells in PIL but not during conventional immunization

A peculiarity of P2X7 among the P2 family of ATP-gated ionic channels is the low affinity for ATP; therefore relatively high concentrations of ATP (µM range) are required for its activation. Under physiological conditions, eATP is virtually absent in tissue interstitia. However, stress, injuries or inflammation considerably enhance the concentration of eATP that acts as a danger-associated molecular pattern. To address whether P2X7-mediated control of Tfh cell expansion was peculiar for the inflammatory and immunopathogenic environment elicited by pristane administration but not immunization with a conventional antigen, we immunized WT and *P2rx7*$^{-/-}$ mice with NP_{16}-OVA in MF59, a potent ATP-releasing adjuvant (Vono et al., 2013; Fig. 4 A). In contrast to the enhanced response to pristane, we detected an impaired expansion of Tfh cells and OVA-peptide$_{329–337}$–specific CD4 cells (Fig. 4 B) as well as NP-specific GC B cells (Fig. 4 C) in the draining lymph nodes of *P2rx7*$^{-/-}$ mice 7 d after immunization. Boost immunization at 14 d and analysis after 7 d showed the persistent reduction of antigen-specific B

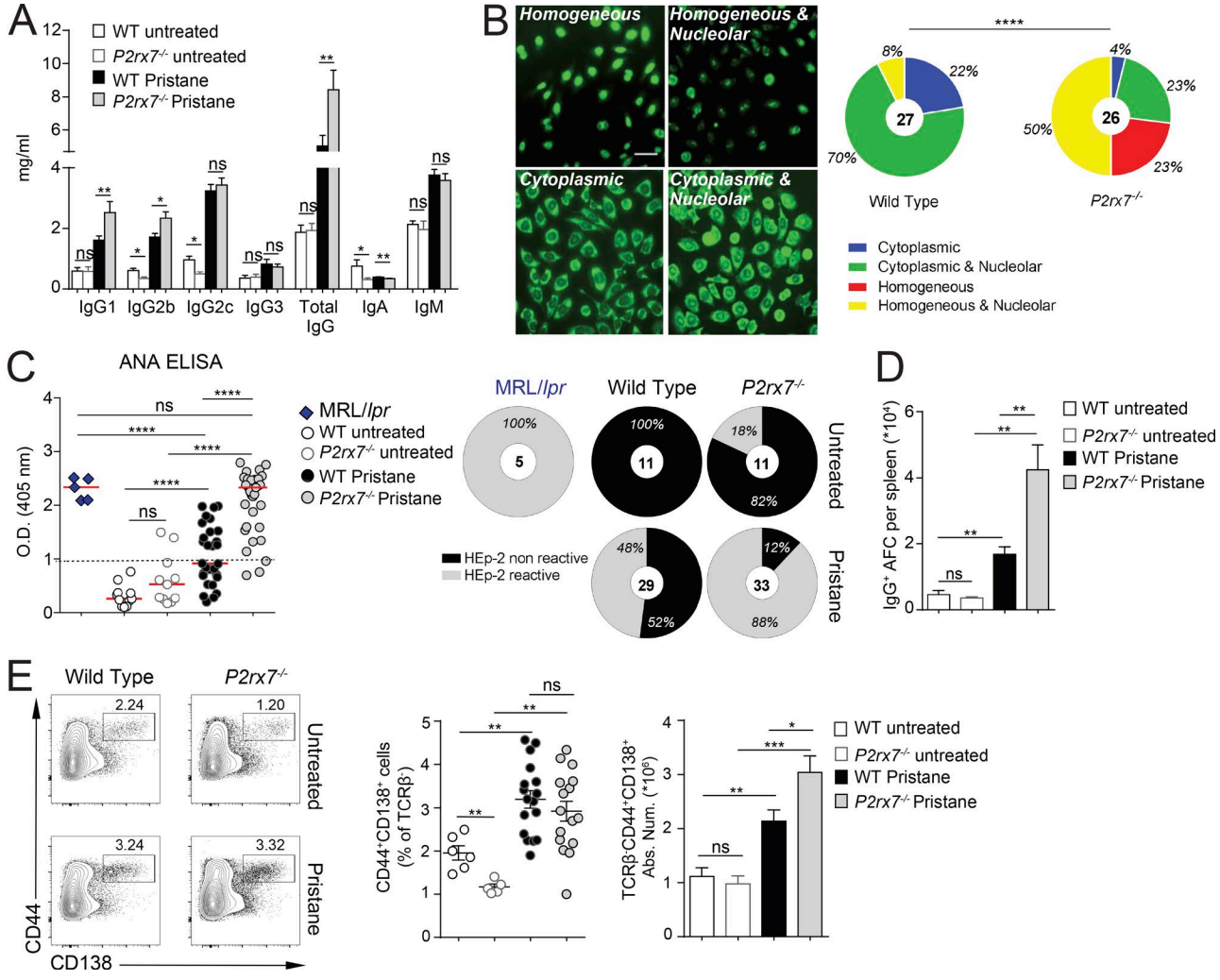

Figure 2. **Increased serum autoantibodies and splenic plasma cells in *P2rx7*$^{-/-}$ mice. (A)** Serum Ig isotype concentrations in untreated (n = 6 for IgM and IgA, n = 16 for total IgG, n = 12 for IgG subclasses) and pristane-treated (n = 15 for IgM and IgA, n = 40 for total IgG, n = 15 for IgG subclasses) mice by ELISA. Mean ± SEM are shown. Two-tailed nonparametric Mann–Whitney U test. **(B)** Representative immunofluorescence of HEp-2 cells and relative distribution of ANA IgG staining patterns with sera from pristane-treated WT and *P2rx7*$^{-/-}$ mice. Bar, 50 µm. The number in the circle indicates the number of analyzed mice. Fisher's exact test with χ^2. **(C)** ELISA (QUANTA-Lite ANA) for the semiquantitative detection of self-reactive IgG. Each dot represents an individual mouse, and horizontal lines represent median values. MRL/*lpr* sera were used as positive controls. MRL/*lpr* (n = 5), WT untreated (n = 11), *P2rx7*$^{-/-}$ untreated (n = 11), WT pristane (n = 29), *P2rx7*$^{-/-}$ pristane (n = 33). Two-tailed Mann–Whitney U test. Distribution of sera from the indicated mice as nonreactive or reactive in the assay is shown. **(D)** Absolute number of IgG-secreting cells by ELISPOT assay in spleens from the indicated mice. Mean ± SEM of three independent experiments. WT untreated (n = 4), *P2rx7*$^{-/-}$ untreated (n = 4), WT pristane (n = 7), *P2rx7*$^{-/-}$ pristane (n = 9). **(E)** Representative contour plots, relative frequency and absolute number of splenic plasma cells gated as TCRβ$^-$CD138$^+$CD44$^+$ cells from untreated WT (n = 6) and *P2rx7*$^{-/-}$ (n = 5) mice and treated WT (n = 17) and *P2rx7*$^{-/-}$ (n = 16) mice. Two-tailed Mann–Whitney U test. Mean ± SEM are shown in bar graphs. *, P < 0.05; **, P < 0.01; ***, P < 0.001; ****, P < 0.0001. ns, not significant.

cells in the spleen of mutant animals (Fig. 4 D) concomitant to significantly reduced abundance of both high- and low-affinity IgG-secreting B cells specific for NP_4 and NP_{41} antigen, respectively (Fig. 4 D). These cells as well as OVA-peptide$_{329–337}$–specific CD4 cells were also significantly reduced in *P2rx7*$^{-/-}$ mice 7 d after subcutaneous injection of NP_{16}-OVA in PBS at day 95 after primary immunization (Fig. 4 E). These results suggest that enhanced GC reaction and hyper-IgG observed in pristane-treated *P2rx7*$^{-/-}$ mice are not general features of the adaptive immune response triggered in the absence of P2X7 but characterize the immunopathogenic response triggered by pristane. Since P2X7 is important in promoting the proinflammatory activation of APCs during antigen priming of adaptive immunity (Wilhelm et al., 2010), the defective antigen responsiveness of *P2rx7*$^{-/-}$ mice could be due to impaired APC activation. To rule out an intrinsic defect of *P2rx7*$^{-/-}$ Tfh cells during antigen priming, we transferred either WT or *P2rx7*$^{-/-}$ TCR transgenic CD90.2 OT-II CD4 cells (specific for OVA peptide 323–339) into congenic CD90.1 WT mice and repeated the immunization with NP_{16}-OVA in MF59. The analysis of primary as well as reactivated memory response revealed undistinguishable frequencies of antigen-specific CD4 cells in mice adoptively transferred with WT or *P2rx7*$^{-/-}$ OT-II cells (Fig. 5 A). Conversely, the transfer of CD90.2 WT or *P2rx7*$^{-/-}$ naive T CD4 cells into congenic CD90.1 WT animals and subsequent injection of pristane (to reproduce the features of experimental lupus within this adoptive transfer system) recapit-

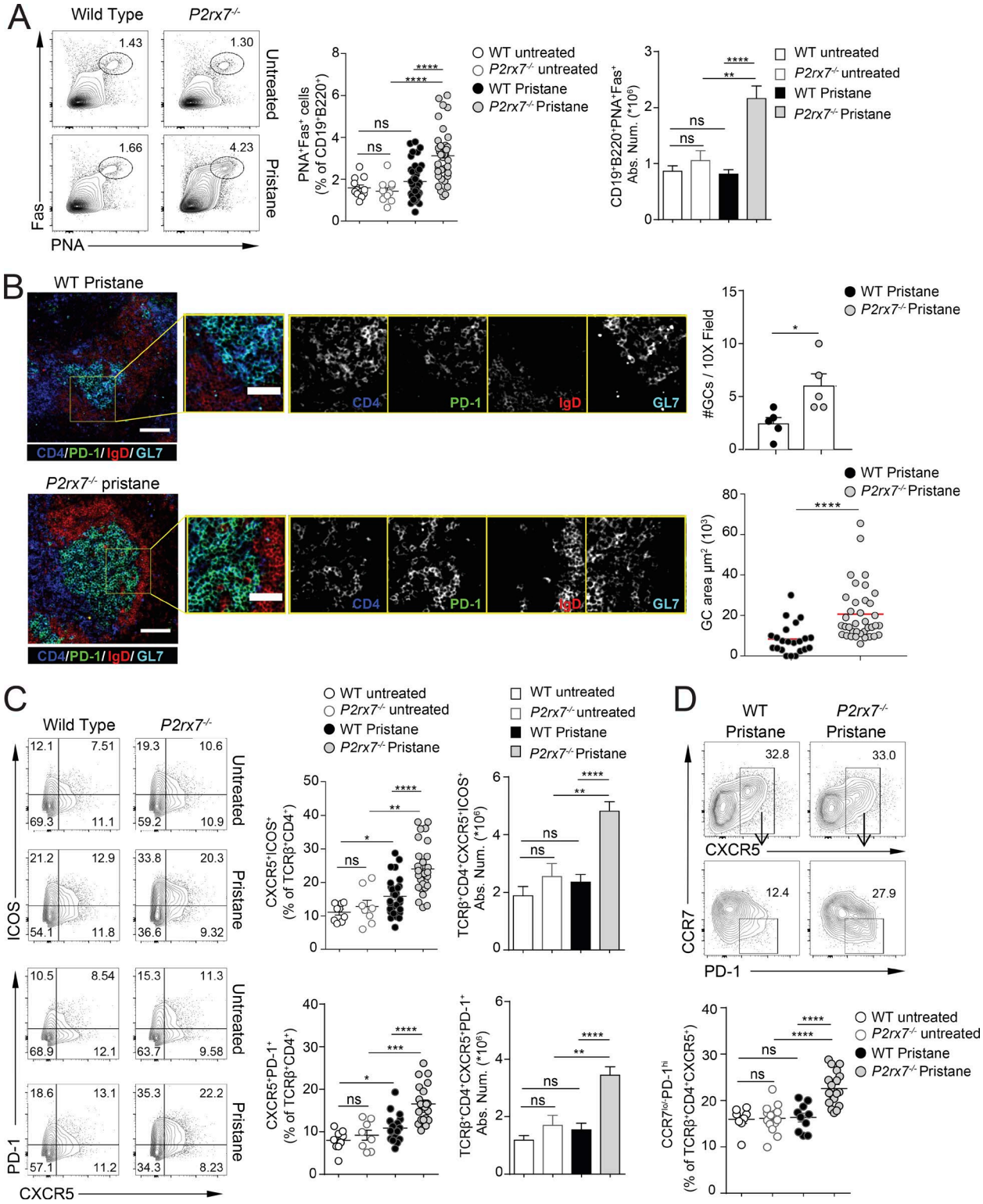

Figure 3. **Increased GC reaction and Tfh cells in *P2rx7*$^{-/-}$ mice. (A)** Representative contour plots for PNA and Fas staining on gated CD19$^+$B220$^+$ splenocytes, and frequency and absolute number in untreated (n = 12) and treated (n = 37) WT as well as *P2rx7*$^{-/-}$ mice. **(B)** Representative images of spleen sections from pristane-treated WT and *P2rx7*$^{-/-}$ mice stained with anti-IgD, -CD4, –GL-7, and –PD-1 antibodies (bar, 100 µm) and inset zooming on GC cells (bar, 50 µm). The number of GCs per field at 10-fold magnification in individual mice (n = 5) and GC areas in WT (n = 22) and *P2rx7*$^{-/-}$ (n = 37) mice are shown in right panels. Two-tailed Mann–Whitney *U* test. Mean ± SEM are shown in bar graphs. **(C)** Representative contour plots and frequency and absolute number of CXCR5$^+$ICOS$^+$ (untreated WT, n = 10; *P2rx7*$^{-/-}$, n = 9; treated WT, n = 30; and *P2rx7*$^{-/-}$, n = 34 mice) and CXCR5$^+$PD-1$^+$ (untreated WT, n = 9; *P2rx7*$^{-/-}$, n = 8; treated WT, n = 17; and *P2rx7*$^{-/-}$, n = 22 mice) cells within gated TCRβ$^+$CD4$^+$ splenocytes. Bar graphs: mean ± SEM. Two-tailed Mann–Whitney *U* test. **(D)** Representative contour plots for CCR7 and PD-1 among CXCR5$^+$ CD4 T cells, and frequency of CCR7$^{lo/-}$PD-1^{hi} CD4 Tfh cells in the spleen of indicated mice. WT untreated (n = 8), *P2rx7*$^{-/-}$ untreated (n = 13), WT pristane (n = 10), *P2rx7*$^{-/-}$ pristane (n = 17). Two-tailed Mann–Whitney *U* test. Each dot in graphs represents an individual mouse, and horizontal lines represent median values. *, P < 0.05; **, P < 0.01; ***, P < 0.001; ****, P < 0.0001. ns, not significant.

ulated the significant increase of donor *P2rx7*$^{-/-}$ compared with WT Tfh cells (Fig. 5 B). Notably, Tfh cell expansion significantly correlated with GC B cell abundance (Fig. 5 C) in the recipient treated hosts. The contrasting data obtained with the two in vivo adoptive transfer models, OVA immunization versus pristane administration, support the hypothesis that P2X7 plays an exquisite role in limiting the expansion of potentially pathogenic Tfh cells upon inflammation and chronic exposure to self-antigens, but its activity does not influence Tfh cell response within vaccination.

P2X7 intrinsically regulates the aberrant generation of Tfh cells and GC-derived autoantibodies

We investigated whether self-reactive IgG induced by pristane originated from a GC-dependent or -independent pathway. To address this issue, first we analyzed the impact of the treatment in *Icos*$^{-/-}$*P2rx7*$^{-/-}$ mice, which are devoid of Tfh cells and cannot generate GCs (Proietti et al., 2014). As expected, in the absence of ICOS-dependent generation of Tfh cells we did not detect variations in GC B cell abundance with respect to untreated animals (Fig. 6 A). Consistent with a pathogenic role of ICOS$^+$ Tfh cells in PIL, *Icos*$^{-/-}$*P2rx7*$^{-/-}$ mice showed significantly reduced self-reactive IgG in serum (Fig. 6 B) and proteinuria (Fig. 6 C) compared with single mutant *P2rx7*$^{-/-}$ mice. Hence, in the absence of Tfh cells and GCs, *P2rx7* deletion in B cells does not apparently influence the generation of pathogenic self-reactive IgG levels as observed in *P2rx7*$^{-/-}$ mice. These data suggest that the proportion of extrafollicular self-reactive IgG accounts only for a minority of the repertoire of autoreactive antibodies generated by pristane injection and that the vast majority of self-reactive IgG detected in the sera from pristane-treated *P2rx7*$^{-/-}$ mice originate from GCs and depend on the presence of P2X7-deficient Tfh cells.

To definitely restrict the function of P2X7 in T cells in limiting the generation of immunopathogenic IgG in a GC-competent host, we repeated PIL in mice with conditional deletion of *P2rx7* in T cells (*Cd4-Cre P2rx7*$^{fl/fl}$). Analogously to *P2rx7*$^{-/-}$, *Cd4-Cre P2rx7*$^{fl/fl}$ mice showed increased Tfh and GC B cells in PPs consistent with impaired regulation of Tfh cells by intestinal ATP (Proietti et al., 2014). When compared with *Cd4-Cre P2rx7*$^{WT/WT}$, these mice recapitulated increased splenomegaly and proteinuria following pristane administration, as previously observed in *P2rx7*$^{-/-}$ versus WT mice (Fig. 1, A and B; and Fig. 7, A and B), suggesting these two phenotypic traits of PIL are influenced by P2X7 in T cells. Aging (33-wk-old) *Cd4-Cre P2rx7*$^{fl/fl}$ mice showed reduced IgG-secreting cells (Fig. 7 E) and GC B cells (Fig. 7 F) in the spleen compared with *Cd4-Cre P2rx7*$^{WT/WT}$ mice. Moreover, serum IgG concentration did not increase upon pristane administration, as observed in *P2rx7*$^{-/-}$ mice (Fig. 7 C). It is possible that this feature of PIL is not T cell intrinsic but depends on the lack of P2X7 in other cells. Moreover, we cannot definitely exclude that the deregulation of other T cell subsets by lack of P2X7 activity might contribute to the phenotype of pristane-treated *Cd4-Cre P2rx7*$^{fl/fl}$ mice. Nonetheless, the significant worsening of selected immunopathological features of SLE, including ANA serum concentration (Fig. 7 D) and IFN-γ–secreting ICOS$^+$ PSGL-1$^{lo/-}$ CD4 cells (Fig. 7 H; see below) in *Cd4-Cre P2rx7*$^{fl/fl}$ mice, together with the observed phenotype of *Icos*$^{-/-}$*P2rx7*$^{-/-}$ animals following pristane administration, suggests that P2X7 activity is crucial in restraining the T cell helper function to B cells bearing self-reactive IgG.

Augmented IFN-γ secretion by PSGL-1$^{lo/-}$ committed Tfh cells in pristane-treated *P2rx7*$^{-/-}$ mice

The lineage-defining transcription factor Bcl6 orchestrates Tfh cell differentiation and function via complex and only partially understood mechanisms (Hatzi et al., 2015). Bcl6-dependent down-regulation of PSGL-1 is part of the Tfh cell differentiation program (Poholek et al., 2010). In MRL/*lpr* mice, ICOS-dependent interaction with B cells was shown to promote PSGL-1 down-regulation and autoantibody production (Odegard et al., 2008). Analogously to these mice, we found a significant increase of PSGL-1$^{lo/-}$ cells in pristane-treated *P2rx7*$^{-/-}$ mice (Fig. 6 D). Concomitant *Icos* deletion abolished PSGL-1 down-regulation (Fig. 6 D), suggesting that ICOS-dependent and protracted functional activity in *P2rx7*$^{-/-}$ cells is responsible for the generation of PSGL-1$^{lo/-}$ committed Tfh cells. Expression of IL-21 is considered a key feature of normal (Nurieva et al., 2008) as well as pathogenic Tfh cells (McGuire et al., 2011; Yang et al., 2013; Kim et al., 2015). However, other proinflammatory cytokines such as IFN-γ (Lee et al., 2012; Domeier et al., 2016; Jackson et al., 2016) or IL-17 (Ding et al., 2013) were implicated in aberrant Tfh cell function. Intracellular staining for IL-21, IL-17, and IFN-γ showed a preferential increase in the percentage of IFN-γ–secreting CD4 cells in pristane-treated *P2rx7*$^{-/-}$ mice (Fig. 6 E) that was abolished by *Icos* deletion (Fig. 7 J). Accordingly, we observed a selective enrichment of IFN-γ–secreting cells in ICOS$^+$ and PSGL-1$^{lo/-}$ CD4 cells (Fig. 7 I). As mentioned above, an analogous enrichment was also observed in mice with conditional deletion of *P2rx7* in CD4 cells (Fig. 7 H). According to previous data showing the relative resistance of *P2rx7*$^{-/-}$ CD4$^+$ T cells to differentiate along the Th17 pathway (Schenk et al., 2011), we detected decreased percentages of IL-17–secreting cells in pristane-treated *P2rx7*$^{-/-}$ mice as well as decreased percentages of IL-21–secreting cells with respect to WT mice (Fig. 7 J). These observations are consistent with the reported role of IFN-γ–secreting Tfh cells in contributing to lupus pathology (Lee et al., 2012).

P2X7-mediated pyroptosis of Tfh cells via caspase-mediated activation of gasdermin D

Online monitoring of cell permeability to YO-PRO-1 by flow cytometry upon stimulation with the P2X7 agonist 3′-*O*-(4-benzoyl) benzoyl ATP (BzATP) is used to assess cellular sensitivity to death mediated by cytolytic pore opening. Tfh cells from spleen of pristane-treated WT but not *P2rx7*$^{-/-}$ mice were sensitive to P2X7 stimulation in this assay (Fig. 8 A). In T cells, P2X7-mediated pore opening and cell death was associated with features characteristic of pyroptosis (Taylor et al., 2008), a form of death executed by gasdermin D (Gsdmd) upon caspase-mediated cleavage and relief of autoinhibition of the pore forming N terminus (Kayagaki et al., 2015; Shi et al., 2015). A search of gene expression profiles in public datasets revealed Gsdmd as the most widely represented member among the gasdermin family in CD4 naive and Tfh cells (Fig. S3 A). In addition, the analysis of caspase expression in CD4 naive versus Tfh cells revealed the selective up-regulation of caspase-1 and -4 in Tfh cells (Fig. S3 B). Since Gsdmd is a sub-

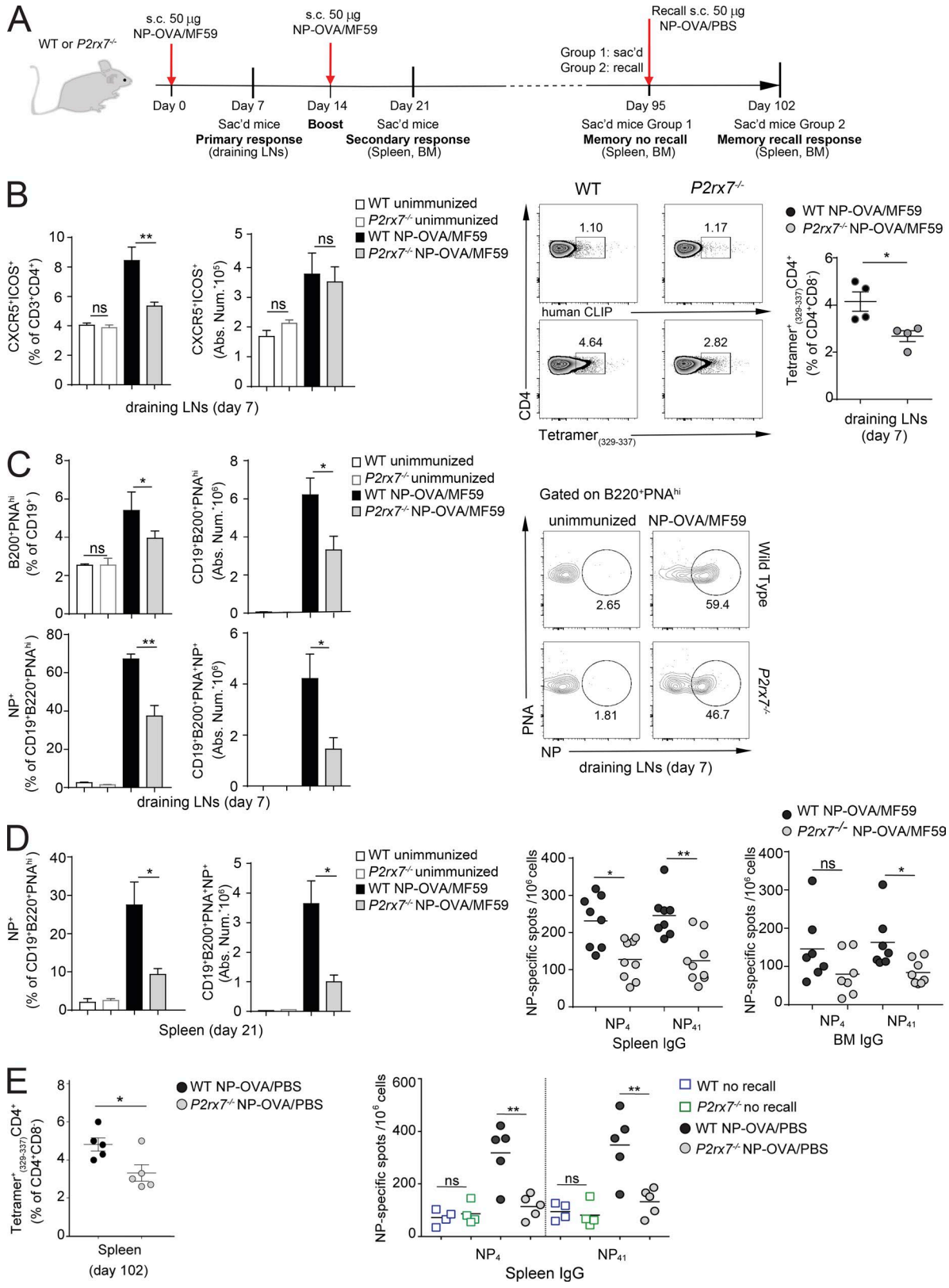

Figure 4. **Impaired primary, secondary, and memory responses to NP-OVA in *P2rx7*$^{-/-}$ mice. (A)** Scheme of the immunization protocol and time points of analysis. **(B)** Frequency and absolute number of CXCR5$^+$ICOS$^+$ Tfh cells in the draining lymph nodes from untreated or immunized WT and *P2rx7*$^{-/-}$ mice at 1 wk after s.c. injection of NP-OVA in MF59 (WT unimmunized, $n = 5$; *P2rx7*$^{-/-}$ unimmunized, $n = 5$; WT NP-OVA, $n = 8$; *P2rx7*$^{-/-}$ NP-OVA, $n = 8$), representative contour plots of staining with human CLIP and OVA tetramers, and statistics of OVA tetramer positive cells ($n = 4$). **(C)** Frequency and absolute number of GC B cells (same samples as above) gated as PNA^{hi}B220$^+$ among CD19$^+$ B cells (upper bar graphs) and of NP-positive GC B cells (lower bar graphs) with representative contour plots. **(D)** Frequency and absolute number of NP-positive GC B cells in the spleen of the indicated mice within secondary response to NP-OVA.

strate of caspase-1 and -4, this observation suggests that Tfh cells could be sensitive to Gsdmd pore-forming activity and execute pyroptosis in Tfh cells upon exposure to BzATP. Accordingly, BzATP stimulation of Tfh cells isolated from pristane-treated WT but not *P2rx7*$^{-/-}$ mice resulted in caspase activation (Fig. 8 B) and generation of cleaved Gsdmd (Fig. 8 C), suggesting that P2X7 limits Tfh cell survival in eATP-rich microenvironment via Gsdmd-mediated pyroptotic cell death.

Phenotypic and functional distinction of circulating Tfh cells in SLE and PAPS donors

As previously shown (He et al., 2013), we observed significantly increased frequencies of the CCR7$^{lo/-}$PD-1^{hi} subset of circulating Tfh (cTfh) cells in our cohort of SLE patients (Table S1 and Fig. 9 A). Interestingly, the analysis of these cells in patients suffering from PAPS did not reveal differences with respect to healthy donors (HDs; Fig. 9 A). Moreover, quantification of CXCL13 in the blood as a Tfh cells derived biomarker of GC activity in humans (Havenar-Daughton et al., 2016) showed the significant increase in SLE but not PAPS with respect to HDs (Fig. 9 B). These results support a role for deregulated Tfh cells in autoantibody generation and pathogenesis in SLE, but not PAPS (where SLE features are not observed even in the presence of antiphospholipid antibodies, including lupus anticoagulant, anti-cardiolipin, or anti-β2-glycoprotein-I antibodies; Ruiz-Irastorza et al., 2010). To investigate possible differences in cTfh cell function in SLE and PAPS, we used a chemokine receptor signature, which classifies these cells into three majors subsets: efficient B cell helper cells, defined as cTfh2 (CXCR3^{-}CCR6^{-}) and cTfh17 (CXCR3^{-}CCR6^{+}) cells, which are increased in some autoimmune disorders, including SLE, and nonefficient B cell helper cTfh1 (CXCR3^{+}CCR6^{-}) cells (Ueno et al., 2015; Blanco et al., 2016). We confirmed a significant increase in cTfh2 and a concomitant decrease in cTfh1 cells in SLE patients. In contrast, PAPS patients were characterized by the increase in a cTfh1/Tfh17 "hybrid" subset that was negatively associated with disease activity in SLE (Choi et al., 2015; Fig. S4 A). SLE and PAPS patients showed an opposite trend of the ratio between the sum of cTfh2 and cTfh17 cells with cTfh1 cells compared with HDs. Whereas SLE patients showed a significant increase of this value, as previously described (Le Coz et al., 2013), PAPS patients displayed a significant reduction, thereby defining a functional distinction of cTfh cells in these two autoantibody-mediated pathological conditions (Fig. S4 B).

Impaired P2X7 receptor activity unleashes Tfh cell expansion in SLE

To address possible differences in sensitivity to eATP via P2X7 in cTfh cells from SLE versus PAPS, we tested YO-PRO-1 permeability in flow cytometry upon stimulation with BzATP. This assay is sensitive in detecting P2X7 activity in human cTfh cells, and preincubation with the P2X7 inhibitor A438079 completely abolished the dye uptake (Fig. S4 C). These experiments revealed the significant reduction of BzATP-sensitive cTfh cells and impairment of YO-PRO-1 permeability in SLE patients with respect to both healthy and PAPS subjects (Fig. 9 C). YO-PRO-1 permeability by P2X7 stimulation inversely correlated with the frequency of CCR7$^{lo/-}$PD-1^{hi} cTfh cells (Fig. 9 D). Principal component analysis (PCA) for the frequencies of CCR7$^{lo/-}$PD-1^{hi} and YO-PRO-1^{+} cells as well as YO-PRO-1 uptake at 450 s identified two main clusters: while HDs and PAPS segregated close to each other, SLE samples were clearly differentiated along the first component (Fig. 9 E). These results indicate that impaired P2X7 activity might be responsible for the increase in cTfh cells in SLE. In line with the reduced sensitivity to pore formation, *P2RX7* mRNA was significantly reduced in cTfh cells from SLE with respect to both healthy and PAPS donors, suggesting that *P2RX7* is selectively down-regulated in SLE (Fig. 10 B). Stimulation of sorted CD4 naive T cells and cTfh cells from HDs with anti-CD3/CD28 antibodies induced progressive up-regulation of *P2RX7* transcripts, which were significantly higher in ex vivo sorted and in vitro activated cTfh compared with naive T cells (Fig. 10 A). This up-regulation is maintained also by shifting cells in medium with IL-2 after 48-h TCR stimulation (Fig. 10 A). The propensity of effector/memory CD4 cells to expand in an antigen-independent fashion can be scored in vitro by the analysis of cell proliferation in response to cytokines (Geginat et al., 2001). Upon stimulation with IL-7 and IL-15, CXCR5^{+} circulating T cells from SLE patients proliferated more robustly than cells isolated from healthy or PAPS subjects and were significantly more resistant to inhibition of proliferation by BzATP (Fig. 10 C). Analogous defective inhibition was observed also in purified CCR7$^{lo/-}$PD-1^{hi} cells (Fig. 10 D).

It was recently shown that CD4 naive T cells can differentiate into Tfh cells and expand in vitro upon exposure to activin A and IL-12 (Locci et al., 2016). The generation and expansion of Tfh cells in this assay was significantly inhibited by the addition of BzATP (Fig. 10 E). However, CD4 cells from SLE donors generated Tfh cells with the same efficiency irrespective of the presence of BzATP, suggesting that Tfh cells in SLE are poised to be defective in sensing eATP as an inflammatory cue that should limit their function (Fig. 10 E). Altogether, these results point to a role for P2X7 as a checkpoint regulator for Tfh cells that appears to be compromised in SLE.

Discussion

The identification of the *sanroque* mutation (that disrupts a repressor of ICOS) in mice unraveled the causal role of deregulated Tfh cells and GCs in developing high titers of autoantibodies and lupus pathology (Vinuesa et al., 2005). We hypothesize that

WT unimmunized (n = 2), *P2rx7*$^{-/-}$ unimmunized (n = 2), WT NP-OVA (n = 4), and *P2rx7*$^{-/-}$ NP-OVA (n = 4). Absolute number of NP-specific IgG secreting cells in the spleen (WT NP-OVA, n = 8; and *P2rx7*$^{-/-}$ NP-OVA, n = 9) and BM (WT NP-OVA, n = 7; and *P2rx7*$^{-/-}$ NP-OVA, n = 8) of immunized mice. **(E)** Frequency of OVA tetramer positive cells among CD4^{+} T cells (n = 5) and absolute number of NP-specific IgG secreting cells in the spleen of the indicated mice. WT and *P2rx7*$^{-/-}$ no recall (n = 4), WT and *P2rx7*$^{-/-}$ NP-OVA (n = 5). Unpaired Student's t test. Each dot in graphs represents an individual mouse, and horizontal lines represent median values. *, P < 0.05; **, P < 0.01. ns, not significant.

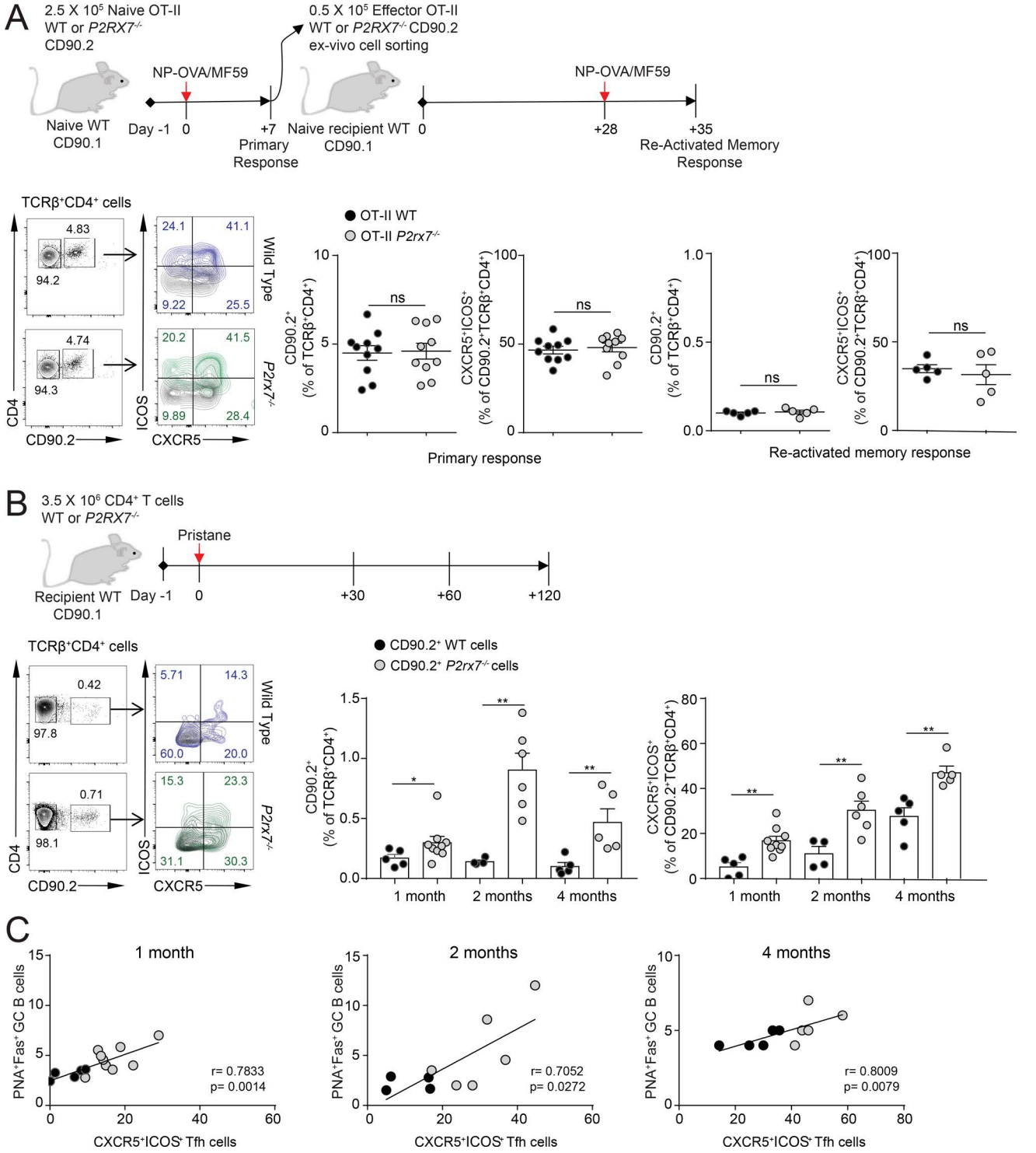

Figure 5. **Selective expansion of *P2rx7*$^{-/-}$ Tfh cells upon pristane injection but not conventional immunization. (A)** Scheme of the adoptive transfer and immunization experiment; representative plots of donor CD4$^+$ and CXCR5$^+$ICOS$^+$ T cells within transgenic cells recovered from the draining lymph nodes of recipient mice 1 wk after primary immunization and frequency of recovered donor cells within individual mice after primary immunization (10 mice per group) and secondary response (five mice per group; mean ± SEM). **(B)** Scheme of the adoptive transfer and pristane administration experiment; representative plots of CD90.2$^+$ donor CD4$^+$ T cells from spleen at 2 mo after transfer, frequency of recovered donor CXCR5$^+$ICOS$^+$ CD4$^+$ T cells within individual mice at 1, 2, and 4 mo after injection of pristane (mean ± SEM). Each dot in graphs represents an individual mouse. Two-tailed Mann–Whitney *U* test. *, P < 0.05; **, P < 0.01. **(C)** Correlation between GC B cells and donor Tfh cell frequencies at the indicated time points. The correlation coefficient r and the respective P value were calculated with nonparametric Spearman test. Each dot in graphs represents an individual mouse.

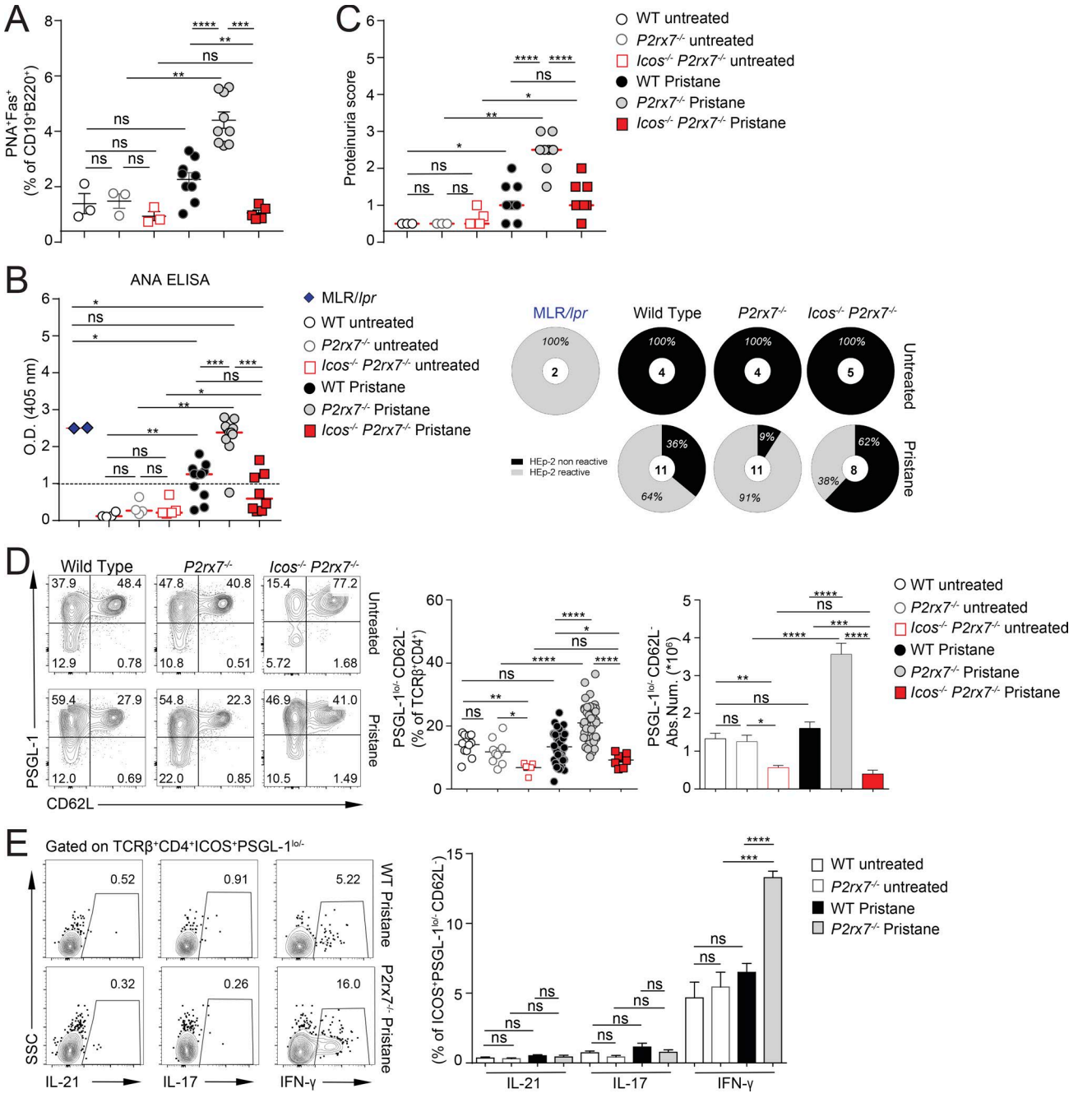

Figure 6. **P2X7-mediated control of PSGL-1 down-regulation and IFN-γ secretion in pristane-treated mice. (A)** Frequency of PNA$^+$Fas$^+$ GC splenic B cells (untreated WT, $n = 3$; *P2rx7*$^{-/-}$, $n = 3$; and *Icos*$^{-/-}$*P2rx7*$^{-/-}$, $n = 3$; pristane-treated WT, $n = 9$; *P2rx7*$^{-/-}$, $n = 9$; and *Icos*$^{-/-}$*P2rx7*$^{-/-}$, $n = 5$). **(B)** Serum ANA IgG detection by ELISA (MRL/*lpr*, $n = 2$; untreated WT, $n = 4$; *P2rx7*$^{-/-}$, $n = 4$; and *Icos*$^{-/-}$*P2rx7*$^{-/-}$, $n = 5$; pristane-treated WT, $n = 9$; *P2rx7*$^{-/-}$, $n = 10$; and *Icos*$^{-/-}$*P2rx7*$^{-/-}$, $n = 10$). **(C)** Proteinuria score (untreated WT, $n = 3$; *P2rx7*$^{-/-}$, $n = 3$; and *Icos*$^{-/-}$*P2rx7*$^{-/-}$, $n = 4$; pristane-treated WT, $n = 8$; *P2rx7*$^{-/-}$, $n = 8$; and *Icos*$^{-/-}$*P2rx7*$^{-/-}$, $n = 8$) in the indicated mice at 33 wk after pristane injection. Each dot represents an individual mouse, and horizontal lines represent median values. **(D)** Representative contour plots for PSGL-1 and CD62L on splenic CD4$^+$ T cells, frequency and absolute number (mean ± SEM) of PSGL1$^{lo/-}$CD62L$^-$ cells from untreated WT ($n = 12$), *P2rx7*$^{-/-}$ ($n = 10$), *Icos*$^{-/-}$*P2rx7*$^{-/-}$ ($n = 5$), treated WT ($n = 38$), *P2rx7*$^{-/-}$ ($n = 37$), and *Icos*$^{-/-}$*P2rx7*$^{-/-}$ ($n = 8$) mice. **(E)** Contour plots show representative intracellular staining for IL-21, IL-17, and IFN-γ on gated CD4$^+$ICOS$^+$PSGL1$^{lo/-}$ cells from spleens of treated WT and *P2rx7*$^{-/-}$ mice. Statistics from three independent experiments are shown (mean ± SEM, untreated mice, $n \geq 4$; treated mice, $n \geq 8$). Two-tailed Mann–Whitney *U* test. *, $P < 0.05$; **, $P < 0.01$; ***, $P < 0.001$; ****, $P < 0.0001$. ns, not significant.

P2X7-mediated regulation of Tfh cells can limit potentially pathogenic GC activity. The abundance of CCR7$^{lo/-}$PD-1^{hi} cTfh cells in the blood correlates with active Tfh cell differentiation (He et al., 2013). These cells were selectively enriched and resistant to P2X7-mediated cell death in SLE but not PAPS patients. Excessive IFN-γ promotes Tfh cell accumulation and lupus-associated pathology (Lee et al., 2012). Our results indicate that P2X7 activity might contribute to inhibition of IFN-γ secretion and offset the

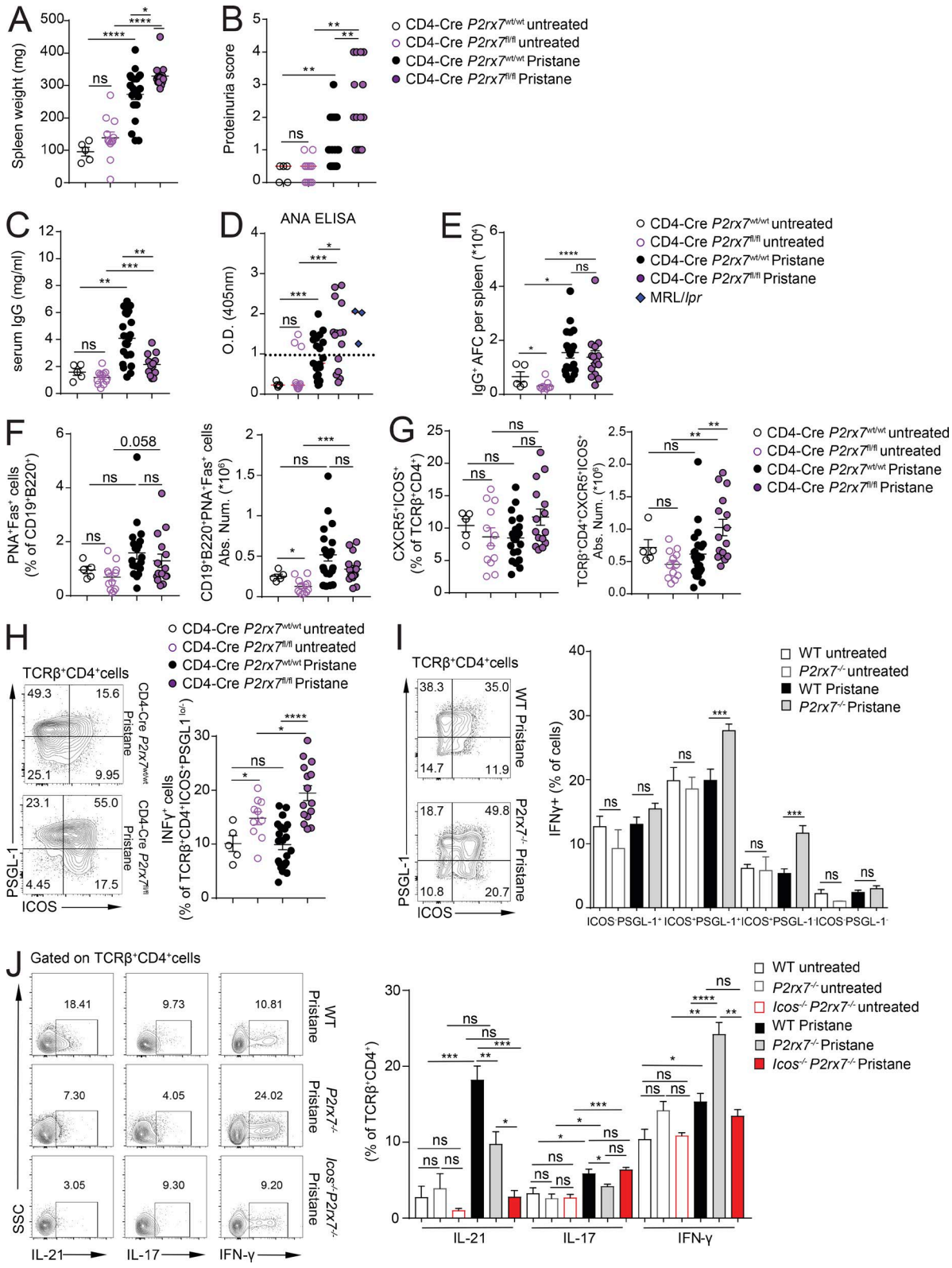

Figure 7. **Increased PIL severity and IFN-γ secretion by ICOS$^+$PSGL-1$^{lo/-}$ CD4 T cells in mice with conditional deletion of *P2rx7* in T cells. (A)** Spleen weight of untreated *CD4-Cre P2rx7$^{WT/WT}$* (n = 5), *CD4-Cre P2rx7$^{fl/fl}$* (n = 12), pristane-treated *CD4-Cre P2rx7$^{WT/WT}$* (n = 21), and *CD4-Cre P2rx7$^{fl/fl}$* (n = 15) mice. **(B)** Proteinuria score. **(C)** Serum IgG concentration. **(D)** Semiquantitative detection of self-reactive IgG by ELISA (QUANTA-Lite ANA) in the same mice. (**E–G**) Absolute numbers of IgG-secreting cells (E) and frequencies and absolute numbers of CD19$^+$B220$^+$PNA$^+$ Fas$^+$ (F) and TCRβ$^+$CD4$^+$CXCR5$^+$ICOS$^+$ (G) cells in the spleen of the same mice. **(H)** Representative contour plots for ICOS and PSGL-1 staining among CD4$^+$ T cells from spleen and frequency of IFN-γ secreting cells within the ICOS$^+$PSGL-1$^{lo/-}$ CD4$^+$ T cells of the same mice. Each dot represents an individual mouse; median or mean ± SEM is shown. Two-tailed Mann–Whitney *U* test. **(I)** Representative contour plots for ICOS and PSGL-1 staining among CD4$^+$ T cells from the spleen of pristane-treated WT and *P2rx7$^{-/-}$* mice,

risk of GC-driven autoimmunity by chronic Tfh cell stimulation. Notably, IFN-γ deficiency did not impair Tfh cell response against immunization with foreign antigen (Lee et al., 2012). According to a dichotomy of P2X7 in regulating Tfh cell function in acute stimulation by cognate antigen versus chronic exposure to inflammatory environments, immunization with OVA did not result in any difference in the expansion of OT-II Tfh cells both in primary and secondary response. Whereas P2X7 activity does not affect Tfh cell response to "physiological" stimulation by exogenous antigens, it appears to limit immunopathological responses. Therefore, restoring P2X7 competence in Tfh cells might improve immunopathology in systemic autoimmunity.

The progressive nature of SLE is characterized by the accumulation of new types of autoantibodies up to the clinical onset of the disease. Moreover, the appearance of specific autoantibodies, namely anti-Sm and anti–nuclear ribonucleoprotein antibodies, tends to coincide with the clinical manifestations of SLE. These observations led to the modeling of disease evolution into three distinct phases of benign autoimmunity, pathogenic autoimmunity, and clinical illness (Arbuckle et al., 2003). The genetic as well as environmental factors influencing the development of pathogenic autoimmunity in SLE are not defined. SLE is a polygenic disease; strong candidates that may cause the disease seem to be located across chromosomal bands 12q24.1 to 12q24.3 (Nath et al., 2004). Together with other potential candidate genes in SLE pathogenesis, *P2RX7* is located within this chromosomal region. Human *P2RX7* is highly polymorphic and contains a large set of single nucleotide polymorphisms that affect P2X7 activity. Haplotypes containing the Ala348>Thr polymorphism (rs1718119) are characterized by a gain-of-function effect (Stokes et al., 2010). Interestingly, this polymorphism was associated with lower risk of SLE in a Chinese population (Chen et al., 2013). CD4 cells from patients with SLE, but not rheumatoid arthritis, exhibited diminished P2X7-dependent ATP-mediated cell death compared with healthy controls (Portales-Cervantes et al., 2010). We have shown a diminished sensitivity of Tfh cells from SLE but not PAPS patients to cytolytic pore opening by P2X7 pharmacological agonist, suggesting that down-regulation of P2X7 might contribute to a selective Tfh cell dysfunction associated with SLE. Notably, aging Fas-deficient MRL/*lpr* mice, which develop a lupus-like syndrome, show a drastically reduced sensitivity to ATP-mediated stimulation of P2X7 in T cells associated with progressive lymphoproliferation (Le Gall et al., 2012). Although we cannot exclude that other mechanisms contribute to the impaired response of Tfh cells to P2X7 stimulation in SLE patients, the observed reduction of *P2RX7* mRNA constitutes a possible cause. This reduction might be correlated to the pronounced changes in microRNAs that characterize SLE and affect lymphocyte function and Ig responses (Zan et al., 2014). In innate immune system, P2X7 has a well-established role as a trigger for inflammatory cytokines release, a feature that fostered the development of P2X7 inhibitors to be used as therapeutic drugs in autoimmune diseases (Ferrari et al., 2006). Our results suggest that P2X7 inhibition in chronic inflammatory conditions where GC activity is enhanced might promote the inappropriate expansion of potentially pathogenic Tfh cells.

Materials and methods

Mice

C57/BL6J, *P2rx7*$^{-/-}$ (B6.129P2-P2rx7tm1Gab/J), *Icos*$^{-/-}$ (B6.129P2-Icostm1Mak/J), OT-II (B6.Cg-Tg(TcraTcrb)425Cbn/J), CD45.1 (B6.SJL-Ptprca Pepcb/BoyJ), CD90.1 (B6.PL-Thy1a/CyJ), and *Cd4-cre* (B6.Cg-Tg(Cd4-cre)1Cwi/BfluJ) mice were from The Jackson Laboratory. The *P2rx7*$^{fl/fl}$ mice were from the European Mouse Mutant Archive (EMMA ID 05116; Skarnes et al., 2011). *Cd4-Cre P2rx7*$^{fl/fl}$ mice were generated by crossing the two strains. All mice were bred in the specific pathogen–free facility at the Institute for Research in Biomedicine (IRB), Bellinzona, Switzerland. All animal experiments were performed in accordance with the Swiss Federal Veterinary Office guidelines and authorized by the Cantonal Veterinary.

PIL

SLE was induced by a single i.p. injection of 0.5 ml pristane to 8-wk-old WT or *P2rx7*$^{-/-}$ female mice. Mice were monitored for clinical signs of SLE until the end of the study (33 wk after dosing) and examined for lesions consistent with SLE by kidney histology and immunofluorescence, presence of serum autoantibodies by ELISA, and cell subsets composition by flow cytometry. Proteinuria was measured using Bayer Albustix reagent strips on collected fresh spots of urine from each mouse. Score from 0 to 4 was applied as follows: 0, none; 1, trace; 2, 30 mg/ml; 3, 100 mg/ml; and 4, ≥500 mg/ml.

Immunization and adoptive transfer of CD4 cells

8-wk-old female mice were s.c. injected with 50 µg of NP_{16}-OVA (BIOSEARCH Technologies) in MF59 (AddaVax; InvivoGen). Draining lymph nodes and spleen were collected 1 wk after injection, and cells were analyzed by flow cytometry. For the analysis of secondary response, the same immunogen was administered at day 14 after primary immunization and cells were analyzed after 1 wk. For analysis at 102 d after primary immunization, 50 µg of NP_{16}-OVA in PBS was administered s.c.; OVA-peptide$_{329–337}$–specific CD4 and NP-specific IgG-secreting spleen cells were quantified 1 wk later. For adoptive transfer of OT-II cells, CD4$^+$ cells were enriched with anti-CD4 coated magnetic beads (Miltenyi Biotec) and sorted as CD4$^+$CD8$^-$CD25$^-$CD44$^-$CD62L$^+$ naive cells on a FACSAria. 8-wk-old CD90.1 mice were injected intravenously with 2.5 × 10^5 sorted cells containing at least 90% OT-II$^+$ cells. Recipient mice were immunized 24 h later with a subcutaneous injection of 50 µg of NP_{16}-OVA (BIOSEARCH Technologies) 1:1 in

and frequency of IFN-γ–secreting cells within the indicated subsets of untreated and treated mice. Statistics from three independent experiments are shown. Mean ± SEM (untreated mice, $n \geq 4$; treated mice, $n \geq 8$). **(J)** Representative contour plots for intracellular staining of IL-21, IL-17, and IFN-γ in CD4$^+$ T cells from spleen of pristane-treated WT, *P2rx7*$^{-/-}$, and *Icos*$^{-/-}$*P2rx7*$^{-/-}$ mice and statistics of frequencies. Mean ± SEM ($n = 2$ independent experiments with at least five mice). Student's *t* test. *, P < 0.05; **, P < 0.01; ***, P < 0.001; ****, P < 0.0001. ns, not significant.

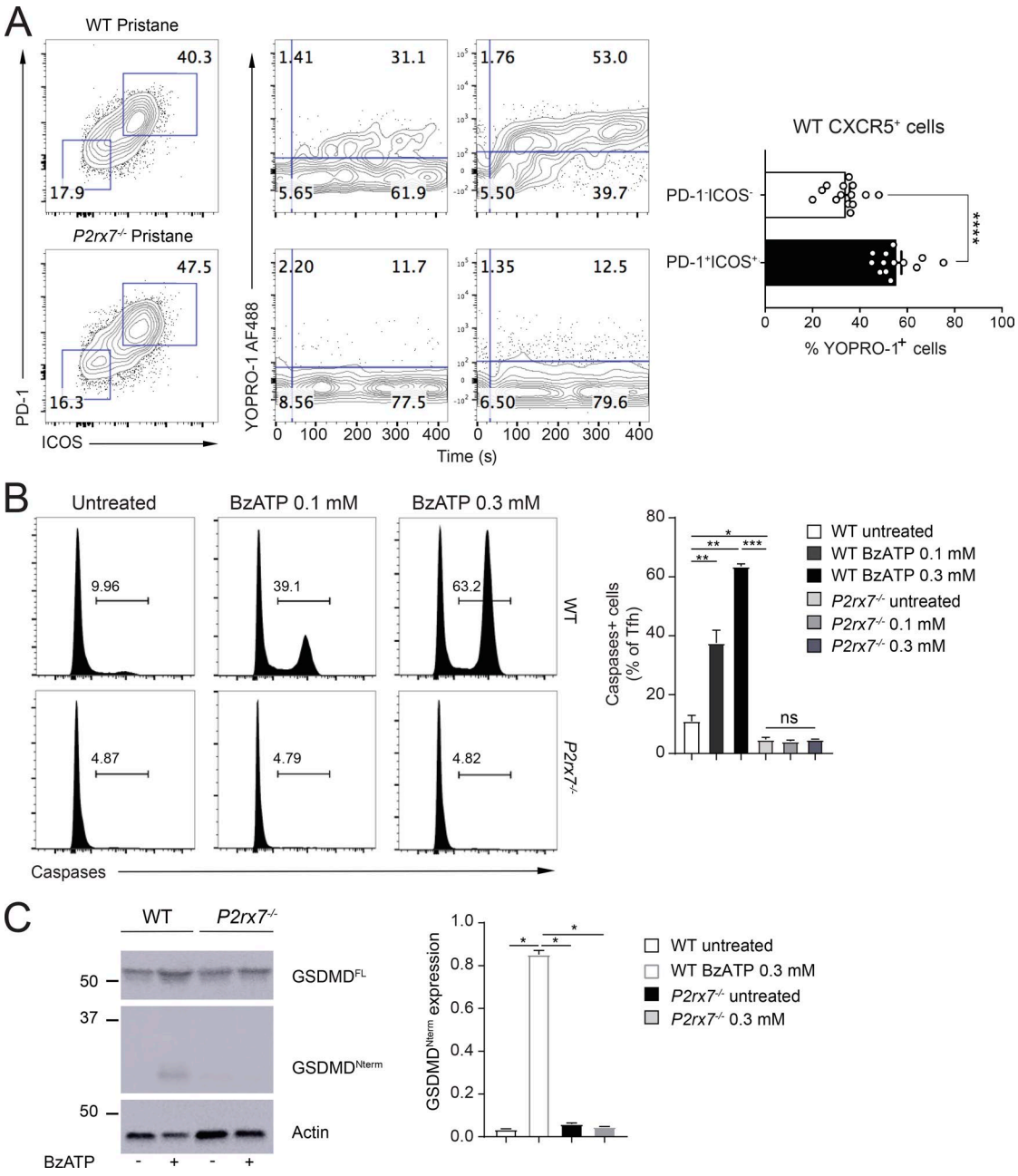

Figure 8. **P2X7-mediated caspase activation and Gsdmd cleavage in Tfh cells. (A)** Time monitoring of YO-PRO-1 uptake after stimulation with BzATP in ICOS⁻PD-1⁻ and ICOS⁺PD-1⁺ cells within CXCR5⁺ CD4⁺ T cells from spleen of WT and *P2rx7*$^{-/-}$ mice at 33 wk after pristane administration and frequency of responding cells in the two subsets from WT mice (n = 14). **(B)** Analysis by flow cytometry and statistics of caspase activation in purified WT and *P2rx7*$^{-/-}$ Tfh cells upon stimulation with BzATP as indicated (n = 4). **(C)** Representative Western blot of full-length and caspase-cleaved Gsdmd (FL and Nterm, respectively), and actin on the same cells as in B, either untreated or stimulated with BzATP. A shorter exposure for $Gsdm^{FL}$ is shown. Histograms show the statistics of $Gsdmd^{Nterm}$ relative expression normalized on $Gsdm^{FL}$ in the indicated conditions (n = 3). Bar graphs: mean ± SEM. Two-tailed Mann–Whitney U test. *, P < 0.05; **, P < 0.01; ***, P < 0.001; ****, P < 0.0001. ns, not significant.

MF59 (AddaVax; InvivoGen). For retransfer of activated OT II effector cells, CD4-enriched cells were sorted for CD90.2 cells, and 5×10^4 cells were injected intravenously into naive CD90.1 hosts. To reactivate memory OT-II cells, recipient mice received a subcutaneous injection of 50 µg of NP_{16}-OVA in MF59 28 d after secondary transfer, and draining lymph nodes were analyzed 1 wk later. For adoptive transfer of polyclonal CD4⁺ T cells from either WT or *P2rx7*$^{-/-}$ mice, spleens were collected, and CD4⁺ cells were enriched with anti-CD4 coated magnetic beads (Miltenyi Biotec) and then sorted as CD4⁺CD8⁻CD19⁻B220⁻CD11c⁻CD11b⁻ cells on a FACSAria. 3.5×10^6 cells were injected into CD90.1 WT mice, and 24 h later, mice were injected i.p. with 0.5 ml pristane. Spleens were collected and analyzed 1, 2, or 4 mo after injection.

Histochemistry and immunohistochemistry

All animals were euthanized with CO_2, followed by exsanguination. For histological evaluation, the kidneys were removed, fixed in 10% neutral buffered formalin for 48 h, trimmed, dehydrated,

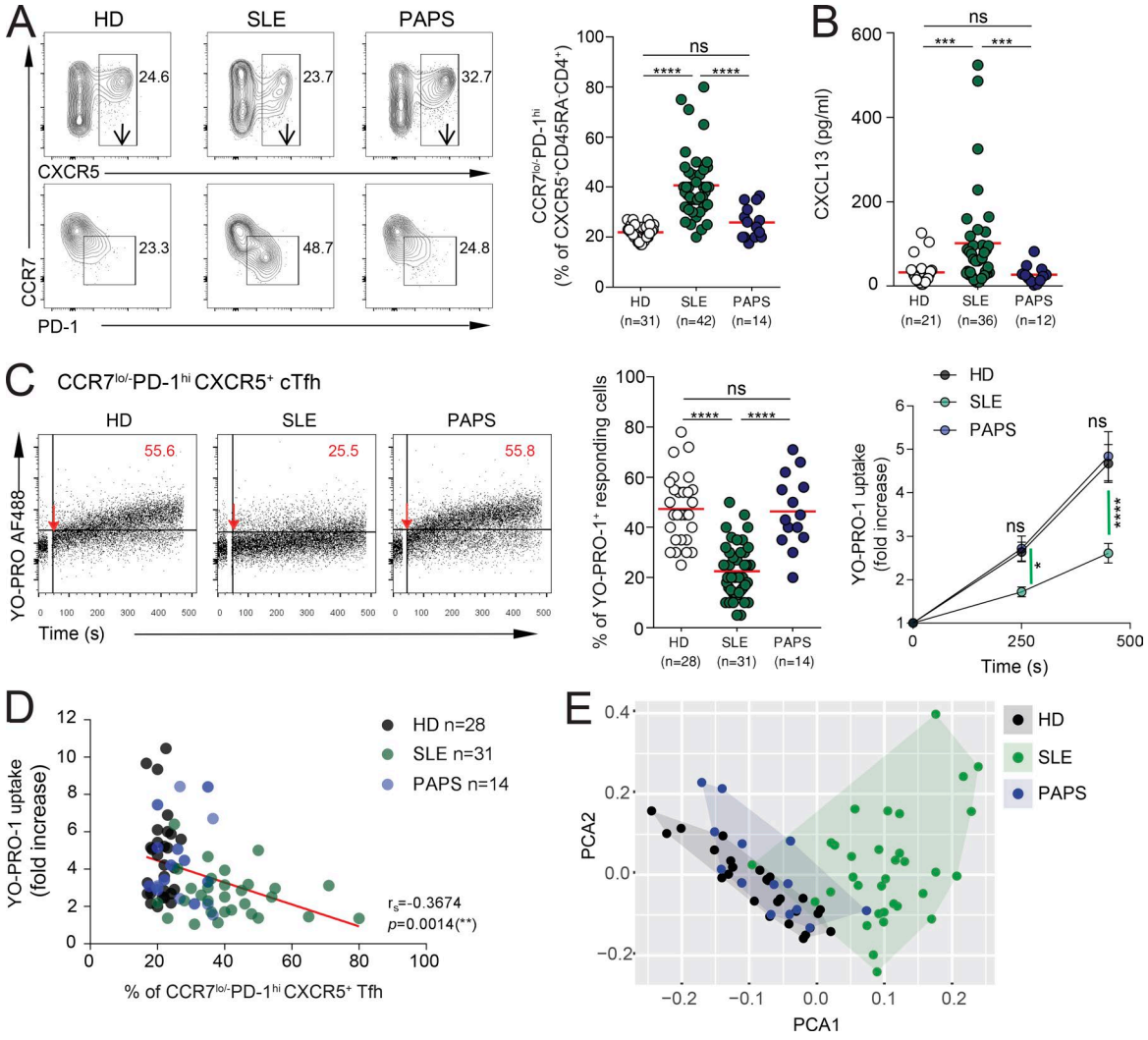

Figure 9. **Frequency of cTfh cells and P2X7 activity in healthy subjects and SLE and PAPS patients. (A)** Representative dot plots for CXCR5$^+$ cells and CCR7$^{lo/-}$PD-1^{hi} cells within cTfh cells of the indicated subjects and frequency of CCR7$^{lo/-}$PD-1^{hi} cells within cTfh cells in healthy (HD), SLE, and PAPS subjects. Two-tailed Mann–Whitney *U* test. **(B)** Serum CXCL13 concentration in HDs, SLE, and PAPS subjects. Two-tailed Mann–Whitney *U* test. **(C)** Representative time monitoring of YO-PRO-1 uptake in CD14$^-$CD4$^+$CD45RA$^-$CXCR5$^+$CCR7$^{lo/-}$PD-1^{hi} cTfh cells from PBMCs of the indicated subjects after stimulation with BzATP. Statistics of YO-PRO-1–permeable cells (two-tailed Mann–Whitney *U* test) and YO-PRO-1 uptake expressed as fold increase of mean fluorescence intensity at 250 and 450 s (two-way ANOVA multiple comparisons, with Bonferroni's correction) are shown. **(D)** Correlation of fold increase in YO-PRO-1 uptake at 450 s and percentage of cTfh cells. The correlation coefficient r and the respective P value were calculated with nonparametric Spearman test. **(E)** PCA of HDs and SLE and PAPS patients according to % cTfh cells, % YO-PRO-1$^+$ cTfh cells, and YO-PRO-1 uptake at 450 s. Areas of spreading are highlighted to better visualize segregation of groups of subjects. Each dot in graphs represents a subject, and horizontal lines represent median values. *, P < 0.05; ***, P < 0.001; ****, P < 0.0001. ns, not significant.

and embedded in paraffin wax. Sections of 3–5-µm thickness were prepared, mounted on glass slides, deparaffinized in xylene, and rehydrated through graded alcohols, before staining with H&E or periodic-acid-Schiff reagent. Slides were evaluated in a blinded fashion by a board-certified veterinary pathologist (G. Pellegrini). Glomerular injury was assessed by light microscopy on 50 consecutive glomeruli/mouse using a histopathological scoring system modified from Wang et al. (1999). Briefly, a grade of 0 indicated normal glomerular histology; scores 1 to 3 indicated progressive severe glomerular injury, i.e., score 1: mildly thickened and hypereosinophilic mesangium, multiple clusters of nuclei, mild reduction in the number of glomerular capillaries; score 2: moderately thickened and hypereosinophilic mesangium, moderate diffuse hypercellularity, marked reduction in the number of glomerular capillaries, occasional inflammatory cells, mostly neutrophils; and score 3: noticeable enlargement of the glomerular tuft, abnormal glomerular shape (irregular rather than round), severely thickened and hypereosinophilic mesangium, occasional adhesions of the glomerular tuft to the Bowman's capsule (synechiae), severe diffuse hypercellularity, loss of capillaries, occasional inflammatory cells, mostly neutrophils. To detect glomerular immune complexes by immunofluorescence, kidneys were removed and immediately frozen in OCT (Tissue-Tek). Cryostat sections (4 µm) were stained with the following antibodies: AF488 goat anti–mouse IgG (highly cross-adsorbed; Southern Biotech), rat anti-mouse C3 (RmC11H9)

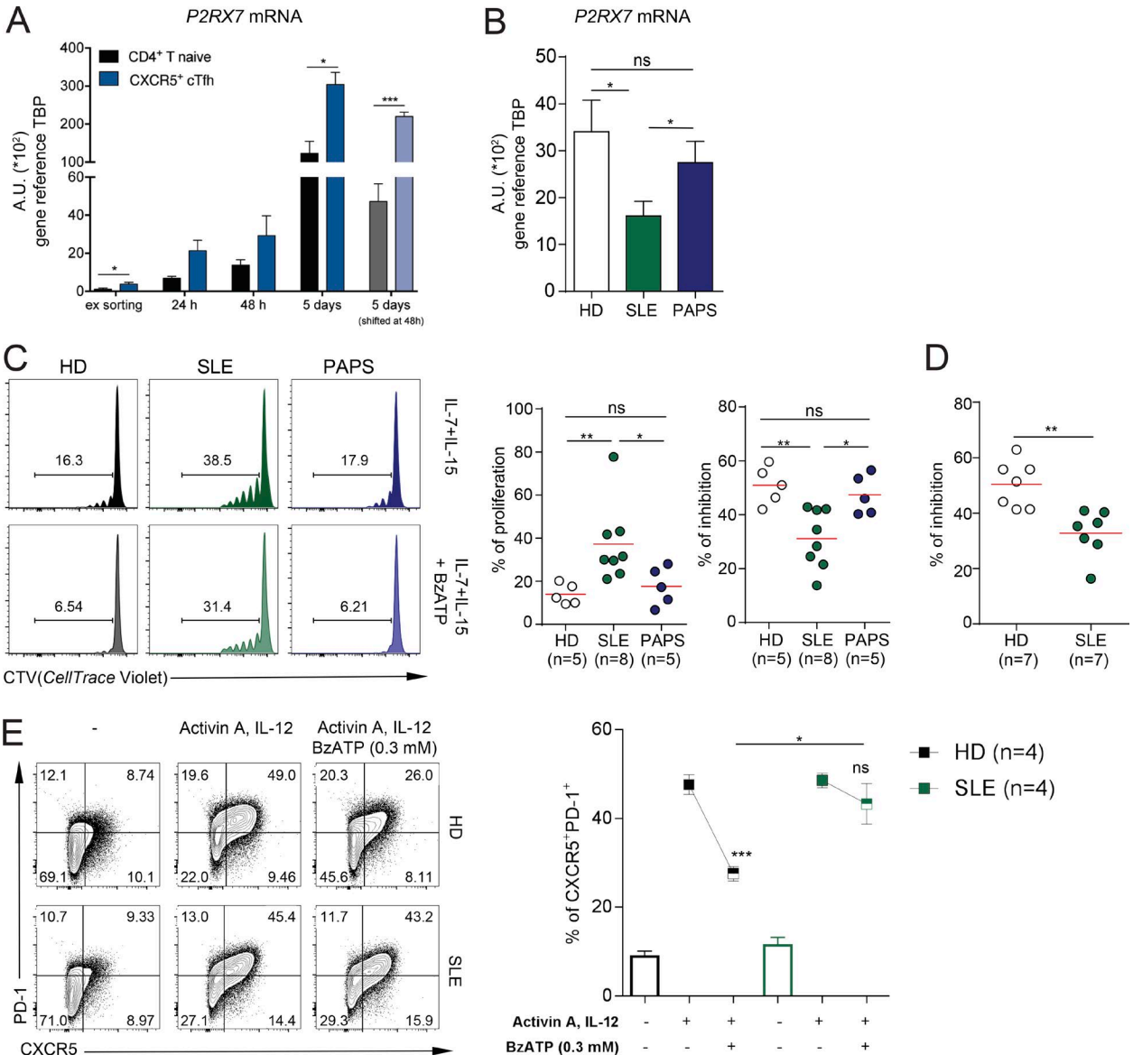

Figure 10. ***P2RX7* expression and function in HDs and SLE and PAPS patients. (A)** *P2RX7* transcript quantification in CD4 naive and cTfh cells at different times after in vitro stimulation with anti-CD3/28 antibodies and upon shifting cells in IL-2 after 48-h stimulation. Data are from cells sorted from three different HDs. Unpaired Student's *t* test. **(B)** *P2RX7* transcripts in sorted CXCR5⁺ CD4 T cells from healthy (HD), SLE, and PAPS donors ($n = 10$). Two-tailed Mann–Whitney *U* test. A.U., arbitrary units. **(C)** Representative histograms of CellTrace Violet (CTV) dilution in purified CXCR5⁺CD4⁺ cells from the indicated subjects after 7-d culture in the presence of IL-7 and IL-15 either without or with BzATP. Percentages of proliferating cells within the marker are indicated. Statistics for proliferation and inhibition of proliferation by BzATP. Each dot represents a subject, and horizontal lines represent median values. Two-tailed Mann–Whitney *U* test. **(D)** Percentage inhibition of proliferation by BzATP in sorted CCR7$^{lo/-}$PD-1^{hi} Tfh cells from HDs and SLE individual subjects at day 7 of stimulation with IL-7 and IL-15. Number of tested donors is indicated in the graphs. Each dot represents a subject, and horizontal lines represent median values. Two-tailed Mann–Whitney *U* test. **(E)** Representative contour plots for in vitro differentiation of naive CD4 cells from HDs and SLE donors ($n = 4$) into Tfh cells in the presence of the indicated stimuli and statistics (Student's *t* test). Bar graphs: mean ± SEM. *, $P < 0.05$; **, $P < 0.01$; ***, $P < 0.001$. ns, not significant.

followed by AF647 labeled goat anti–rat IgG (cross-adsorbed against mouse IgG; Southern Biotech). To detect renal infiltrating CD4 T lymphocytes, the following antibodies were applied to the sections: rat anti-mouse CD4 (clone: GK1.5; BD PharMingen) followed by AF488 goat anti–rat IgG (Invitrogen), hamster anti-mouse ICOS (clone: C398.4A; eBioscience) followed by AF594 goat anti–hamster IgG (Invitrogen). Slides were mounted with Gelvatol Mounting Media and stained with DAPI for the detection of nuclei. Images were acquired using a Leica TCS SP5 confocal microscope, with a HCX PL APO 40×/1.25 N.A. oil-immersion objective. Quantification was performed with ImageJ open-source software (National Institutes of Health; Schindelin et al., 2012). Regions of interest containing the glomeruli were manually defined, and the background was excluded by applying a threshold on the intensity; the area above the threshold in these regions of interest was measured in three different fields of view for each sample and is expressed as percentage of the total glomerulus area. For histological analysis of GCs, spleens were frozen in OCT. Cryostat sections (4 µm) were stained with the following antibodies: AF594 anti–mouse IgD (clone: 11-26c.2a; BioLegend),

AF647 anti-mouse GL-7 (clone: GL-7; BioLegend), BV405 anti-mouse CD4 (clone: GK1.5; BioLegend), unconjugated goat anti-mouse PD-1 Ig (Novusbio) followed by AF488 rabbit anti–goat Ig (Invitrogen). Images were collected on a laser-scanning confocal microscope with a HCX PL APO 40×/1.25 N.A. oil-immersion objective. GC area was measured using ImageJ (Schindelin et al., 2012). To score GC frequency, total GC numbers were quantitated in three separate 10× fields of view of 2.4 mm^2 (1,550 µm × 1,550 µm) per spleen section.

Preparation of single-cell suspension from kidney

Kidneys were removed, minced, and digested with Liberase (0.14 mg/ml; Roche) and DNase I (0.03 mg/ml; Sigma-Aldrich) in HBSS medium, for 30–40 min at 37°C. Tissue pieces were then pressed through a 70-µm strainer to obtain single-cell suspensions. Cells were enriched in leukocytes using an 80/20 Percoll gradient and centrifuged at 800 *g* for 20 min at room temperature. Lymphoid fractions were collected at the interphase of the Percoll gradient and used for flow cytometry.

Mouse cell isolation and flow cytometry

Single-cell suspensions were prepared by passing spleens through a 70-µm nylon mesh. After centrifugation at 1,500 rpm for 5 min, red blood cells were lysed in ACK-lysis buffer for 7 min. Lysis buffer was neutralized by washing once in staining buffer. Cells were stained with the following monoclonal antibodies: biotin-conjugated anti-CXCR5 (clone: 2G8; BD), PE-labeled anti ICOS (clone: 7E.17G9; BD) or PerCPCy5-labeled anti-ICOS (clone: C398.4A; BioLegend), APC-labeled anti PD-1 (clone: RMPI-30; BioLegend), Percp-eFluor710–labeled anti-CD3 (Clone: 17A2; eBioscience), AF488-labeled TCRβ (clone: H57-597; BioLegend), APC-Cy7–labeled anti-CD4 (clone: RM4-5; BioLegend), BV421 anti-CD162 (PSGL1; clone 2PH1; BD), PeCy7-labeled anti-CD25 (clone: PC61; BioLegend), PE-labeled anti-CD44 (clone: IM7; BioLegend), APC-labeled CD62L (clone: MEL-14; eBioscience), and BV421-labeled anti-CD197 (CCR7; clone: 4B12; BioLegend), APC-Cy7–labeled anti-CD19 (clone: 6D5; BioLegend), BV405-labeled B220 (clone: RA3-6B2; BioLegend), PE-labeled anti-Fas (clone: Jo2; BD), fluorescein-labeled peanut agglutinin (PNA; FL-10-71; Vectorlabs), biotinylated anti-CD275 (ICOSL; clone: HK5.3; BioLegend), PE-labeled anti-CD138 (clone: 281-2; BD), APC-labeled anti-CD11c (clone: N418; eBioscience), APC-eFluor780–labeled CD45.2 (clone: 104; eBioscience), and APC-Cy7–labeled anti-CD90.2 (clone: 30-H12; BioLegend). APC-labeled streptavidin was purchased from BioLegend and efluo405-labeled streptavidin from eBioscience. Intracellular staining was performed using the BD Cytofix/Cytoperm and Perm/Wash buffers or, for intracellular FoxP3 (FITC-labeled, clone: FJK-16s; eBioscience) staining, the eBioscience FoxP3 staining buffer set. For intracellular staining of IL-21 (R&D Systems), IFN-γ (PeCy7-labeled, clone: XMG1.2; eBioscience), and IL-17A (PerCP-Cy5–labeled, clone: eBio17B7; eBioscience), 5 × 10^6 splenocytes were cultured for 5 h at 37°C in 24-well plates in 2 ml culture medium containing ionomycin (750 ng/ml) and PMA (20 ng/ml). For the last 4 h, Monensin (1,000× solution; eBioscience) was added to the cultures. IL-21 was detected with a recombinant mouse IL-21R subunit/human IgG1 Fc chimera (R&D Systems) with goat anti-human Fcγ conjugated to AF488 (Jackson ImmunoResearch). For detection of activated caspases, Tfh cells were incubated with FITC-VAD-FMK (CaspGlow Fluorescein Active Caspase Staining Kit; BioVision) for 30–45 min at 37°C in RPMI-1640 according to the manufacturer's protocol. Cells were then washed and resuspended in PBS for analysis by flow cytometry. Samples were acquired on an LSRFortessa (BD Biosciences) flow cytometer. Data were analyzed using FlowJo software (TreeStar).

Tetramer staining

Tetramers were provided by the National Institutes of Health Tetramer Core Facility. Cells were stained for 2 h at 37°C with the following APC-labeled tetramers: I-A^b chicken $OVA_{329–337}$ AAH AEINEA, I-A^b chicken $OVA_{328–337}$ HAAHAEINEA, I-A^b chicken $OVA_{259–277}$ IINFEKLTEWTSSNVMEER, and I-A^b human $CLIP_{87–101}$ PVSKMRMATPLLMQA. All OVA tetramers gave comparable results in flow cytometry.

ELISA and ELISPOT assays

For total Ig isotype determination, ELISA plates (Corning 96-Well Half Area Flat Bottom Polystyrene High Bind) were coated for 3 h at room temperature with purified goat anti–mouse IgG, IgM, and IgA antibodies (Southern Biotech) used at a concentration of 10 µg/ml. After four washes with PBS 0.025% Tween-20 and blocking with PBS 1% BSA for 1 h at room temperature, samples and standards (relative unlabeled mouse Ig; Southern Biotech) were diluted and incubated at room temperature for 4 h. Specific secondary goat anti–mouse Ig conjugated with alkaline-phosphatase were added after four washes with PBS and 0.025% Tween-20 and incubated for 2 h at room temperature. Plates were washed again, and the assay was developed with Sigma 104 phosphatase substrate. Plates were read at 405 nm. IgG-secreting cells were detected using ELISPOT assay: 96-well plates (Millipore, MSIPS4510 Sterile, hydrophobic high protein binding Immobilon-P membrane) were coated with 10 µg/ml purified goat anti–mouse IgG (Southern Biotech) for 2 h at room temperature. After three washes with PBS solution, plates were blocked with PBS and 1% BSA and incubated for 30 min at 37°C. Serial dilutions of splenocytes were added in a final volume of 200 µl B cell medium (RPMI, 10% Hyclone serum) and left at 37°C for 16 h. Subsequently, plates were washed three times with PBS and 0.25% Tween-20 and four times with PBS and incubated for 2 h at room temperature with biotinylated goat anti–mouse IgG (Southern Biotech). After washing, avidin-peroxidase (HRP; Sigma-Aldrich) was added and left for 1 h at room temperature. The assay was developed with AEC (Sigma-Aldrich). For quantification of IgG-secreting cells, plates were acquired, counted, and quality controlled using an ELISPOT reader and ImmunoSpot 5.1 software (CTL Europe). For ANA detection, both indirect immunofluorescence assay ANA-Hep-2 fixed cells (ORG 870; Orgentec) and microwell ELISA plates coated with highly purified individual antigens plus extracts from Hep-2 nuclei and nucleoli (QUANTA Lite; Inova Diagnostics) were used. Briefly, fixed Hep-2 cells were incubated with mouse sera (diluted 1:100), and ANAs were detected with AF488-labeled goat anti–mouse IgG (Southern Biotech). Slides were stained with DAPI and captured with a

Nikon Eclipse E800 upright microscope, with a 20×/0.75 N.A. objective. Images were analyzed with ImageJ open-source software for pattern recognition (Schindelin et al., 2012). The kit ELISA (QUANTA Lite) for the semiquantitative detection of ANAs in human serum was used and adapted for the detection of mouse ANAs. The antigens include chromatin (double-stranded DNA [dsDNA] and histones), Sm/RNP, SS-A, SS-B, Scl-70, centromere, PCNA, Jo-1, mitochondria (M-2), and ribosomal-P protein, as well as the extracts. Sera were diluted at 1:200 in ANA sample diluent and detected with HRP-conjugated goat anti–mouse IgG (Southern Biotech). Plates were read for the absorbance at 450 nm within 1 h after addition of the stop solution.

Western blot

Tfh cells were isolated from mesenteric lymph nodes and PPs, washed with ice-cold PBS, and lysed with RIPA buffer 1× (Sigma) supplemented with protease inhibitor cocktail (Roche). Samples were centrifuged at 14,000 rpm for 10 min at 4°C and snap frozen. Cleared protein lysate was denatured with loading buffer supplemented with 0.1 µM DTT for 10 min at 65°C. Samples were run on precast 4–12% bis-Tris protein gels (Bio-Rad) and then transferred onto polyvinylidene difluoride membranes using Trans-Blot Turbo Transfer System (Bio-Rad). Membranes were blocked with 10% (wt/vol) nonfat dry milk (Bio-Rad) and 0.1% Tween-20 in TBS and incubated with appropriate antibodies in TBS with 0.1% Tween-20 for 16 h at 4°C. The following antibodies were used: anti-GSDMDC1 (clone: A-7, sc-393656; Santa Cruz Biotechnology) and anti-actin (A2066; Sigma). Bound antibodies were revealed by incubation with secondary HRP-conjugated anti-mouse (7076, Cell Signaling Technology) or anti-rabbit (7074; Cell Signaling Technology) IgG antibodies in TBS with 0.1% Tween-20. Membranes were developed using the Pierce ECL Western blotting substrate (32209; Thermo Scientific), signals were detected with the ImageQuant LAS 4000 system in the standard acquisition mode (GE Healthcare Life Sciences), and bands were quantified using the Multi Gauge Analysis tool (Fujifilm).

Human samples and patients

Peripheral blood samples from patients with SLE and PAPS were obtained after informed consent was provided (local ethics committee approval no. 192_2016bis) during regular follow-up visits at the Lupus Clinic, IASST-Istituto Gaetano Pini, University of Milan, Italy. Inclusion criteria were age >18 yr, fulfillment of the American College of Rheumatology 1997 classification criteria for SLE (Hochberg, 1997) and 2006 classification criteria for antiphospholipid syndrome (APS; Miyakis et al., 2006; Table S1). Exclusion criteria were treatment with B cell–depleting agents or experimental drugs. Disease activity was determined with SLE disease activity index (SLEDAI-2K; Gladman et al., 2002); clinical and laboratory data were obtained during the routine follow-up. Patients were characterized for antiphospholipid antibodies (Lupus Anticoagulant, anticardiolipin IgG and IgM, and anti-β2GPI IgG and IgM; Andreoli et al., 2015) as well as ANA, anti-ENA, and anti-dsDNA antibodies (Ingegnoli et al., 2014). All experiments performed on human blood samples from HDs were approved by the ethics committee of Fondazione IRCCS Ca' Granda Ospedale Maggiore Policlinico, and informed consent was obtained from all subjects.

Human cell isolation, stimulation, and flow cytometry

Peripheral blood mononuclear cells (PBMCs) were isolated from blood by density-gradient centrifugation using Ficoll-Paque Plus gradient (GE Healthcare). $CD4^+$ T cells were enriched by positive selection using human CD4 MicroBeads (Miltenyi Biotec), and then $CD4^+$ T cell subsets were sorted to 99% purity with a FACSAria (BD). For in vitro TCR stimulation, $CD4^+$ naive and $CXCR5^+$ cells were stimulated with anti-CD3 (5 µg/ml) and anti-CD28 (1 µg/ml) mAbs. PBMCs were stained with the following antibodies: PE-Texas Red–labeled anti-CD4 (clone: MHCD0417; Life Technologies), QD655-labeled anti-CD45RA (clone: MEM-56; Life Technologies), PE-labeled anti-CCR7 (clone: G043H7; BioLegend), purified mouse monoclonal IgG_{2b} anti-CXCR5 (BRL-1, clone: 51505; R&D Systems) revealed by FITC-labeled anti–mouse IgG_{2b} (Southern Biotech), PE-cyanine 5 (PeCy5)–labeled anti-CD183 (CXCR3; clone: 1C6/CXCR3; BD), PE-labeled anti-CD196 (CCR6; clone: 11A9; BD), BV785-labeled anti-CD279 (PD-1; clone: EH12.2H7; BioLegend). PeCy5-labeled anti-CD56 (clone: A07789; Beckman Coulter), anti-CD14 (clone: A07765; Beckman Coulter), anti-CD19 (clone: HIB19; BioLegend), anti-CD25 (clone: BC96; BioLegend), and anti-CD8 (clone: HIT8a; BioLegend) were included as a dump channel to exclude contaminant cells.

Time monitoring of YO-PRO-1 uptake

10^6 human PBMCs were stained with the appropriate antibodies, washed, resuspended in RPMI 1640 complete medium, and loaded with YO-PRO-1 iodide (Life Technologies) at a final concentration of 5 µM. The YO-PRO-1 uptake following cell stimulation with 1 mM BzATP (Sigma) was monitored on an LSRFortessa for 480 s, and the kinetics was analyzed using FlowJo software (TreeStar). Murine splenocytes (10^6) were stimulated with 0.1 mM BzATP.

In vitro cytokine-driven proliferation assay

For cytokine-driven proliferation assay, sorted $CXCR5^+$ or $CCR7^{lo/-}PD\text{-}1^{hi}$ CD4 T cells were labeled with 5 µM Cell Trace Violet (Life Technologies) in PBS for 20 min at 37°C; staining was blocked by adding an equal volume of filtered prewarmed FBS. Cells were centrifuged at 1,500 rpm for 5 min and plated at a minimal density of 25,000 cells/well in RMPI 1640 complete medium. Plated cells were stimulated with recombinant IL-7 and IL-15 (R&D Systems) at 25 ng/ml, with BzATP at a final concentration of 100 µM when indicated. Cell proliferation and viability were assessed after 7 d using LSRFortessa.

In vitro CD4 cell differentiation to Tfh cell

$CD4^+$ cells were enriched from PBMCs by positive selection with anti-CD4 MicroBeads (Miltenyi Biotec). Naive T cells were sorted on a FACSAria (BD) to 99% purity as $CD8^-CD25^-CD14^-CD19^-CD4^+CD45RA^+CCR7^+$ cells, activated by Dynabeads Human T-Activator CD3/CD28 (Life Technologies), and cultured with recombinant activin A (100 ng/ml), human IL-12 (5 ng/ml), IL-7 (4 ng/ml; all from R&D Systems), and BzATP where indicated, in AIM-V medium (Life Technologies), as described (Locci et al.,

2016). After 5 d, cells were stained with Zombie Aqua dye (BioLegend) to exclude dead cells, anti-human CXCR5, and PD-1 antibodies and analyzed on an LSRFortessa.

Real-time quantitative PCR

CXCR5$^+$ CD4 cells were sorted on a FACSAria (BD) from PBMCs. RNA was extracted using the RNeasy Mini Kit (Qiagen) and converted to cDNA. Random primers and Moloney murine leukemia virus reverse transcription (Invitrogen) were used for cDNA synthesis. Transcripts were quantified by real-time quantitative PCR on an ABI PRISM 7900HT with Applied Biosystem predesigned TaqMan gene expression assays and reagents according to the manufacturer's instructions. The following probe was used (identified by Applied Biosystem assay identification number): *P2RX7* (Hs00175721_m1). For each sample, mRNA abundance was normalized to the amount of TAT-box binding protein (Hs00427620_m1), used as gene reference, and expressed as arbitrary units.

Meta-analysis of gene expression data in CD4 cells

All data were measured on Affymetrix arrays and have been downloaded from the Gene Expression Omnibus (GEO). The following series of GEO data were used: GSE46892 (Huang et al., 2014), GSE49314 (Weber et al., 2015), GSE56883 (Moriyama et al., 2014), GSE21381 (Yusuf et al., 2010), and GSE24574 (Kitano et al., 2011). Microarray probe fluorescence signals were converted to log2 expression values using the Robust Multiarray Average procedure (Irizarry et al., 2003) of the affy Bioconductor package. Fluorescence intensities were background-adjusted and normalized using quantile normalization, and expression values were calculated using median polish summarization and custom chip definition files for a total of 18,139 custom probe sets for Mouse Genome 430 2.0 Array based on Entrez genes (Mouse4302_Mm_ENTREZG version 21.0.0). All data analyses were performed in R version 3.3.3 using Bioconductor libraries and R statistical packages. The expression change of any caspase was quantified as the difference between its log2 expression level in any sample of Tfh cells and its average log2 gene expression signal in naive CD4 cells (log2 fold-change).

PCA

PCA was performed using the "prcomp{stats}" method in R and visualized with ggplot2 library. Datasets were pruned for missing values before analysis; thus a total of 77 samples were used for PCA (28 HD, 14 PAPS, and 35 SLE). The percent contributions of each variable to the segregation process were determined as cumulative sum of absolute values of the PCA loadings, which are an estimate of how much each variable used in the PCA analysis contribute to each of the new variables (the principal components) after the PCA transformation.

Statistical analysis

Statistical analysis was performed with Prism software (GraphPad). Results were analyzed using the nonparametric Mann–Whitney test, Student's unpaired *t* test, and two-way ANOVA with Bonferroni posttest analysis, as indicated. Results are presented as mean ± SEM. Values of P were indicated throughout as *, $P < 0.05$; **, $P < 0.01$; ***, $P < 0.001$; and ****, $P < 0.0001$.

Online supplemental material

Fig. S1 shows the phenotypic analysis of B cells, the distribution of CD4$^+$ T cells for CD44 and CD62L, and frequencies of T reg and Tfr cells in untreated and pristane-treated WT and *P2rx7*$^{-/-}$ mice. Fig. S2 shows the increase of ICOS$^+$ CD4 T cells in kidneys of pristane-treated *P2rx7*$^{-/-}$ mice. Fig. S3 shows gasdermin and caspase expression in CD4 and Tfh cells. Fig. S4 shows the distribution of functional cTfh cell subsets and the ratio of (cTfh17 + cTfh2) with cTfh1 cells in HDs,SLE, and PAPS patients, and YO-PRO-1 uptake inhibition in cTfh cells by A438079. Table S1 lists the demographic, clinical, and laboratory characteristics of SLE and PAPS patients and HDs.

Acknowledgments

We thank David Jarrossay (IRB) for cell sorting and helpful discussion, Rocco D'Antuono (IRB) for help with confocal microscopy and generation of images, Bianca Calí (University of Padua, Italy) for advice on immunofluorescence and discussion, and the National Institutes of Health Tetramer Core Facility for providing tetramers.

This work was supported by the Swiss National Science Foundation (grant 310030-159491), Novartis Stiftung für medizinisch-biologische Forschung (grant 18B096), and a grant from Fondazione per la Ricerca sulla Trasfusione e sui Trapianti to F. Grassi. The fellowship of R. Gualtierotti was supported by Società Italiana di Reumatologia. The PhD fellowship of L. Perruzza was supported by Signora Alessandra.

The authors declare no competing financial interests.

Author contributions: F. Grassi, C.E. Faliti, E. Traggiai, and P.L. Meroni designed experiments. C.E. Faliti performed most experiments. E. Rottoli, L. Perruzza, A. Romagnani, and B. De Ponte Conti performed experiments. M. Idzko contributed *Cd4-Cre P2rx7*$^{fl/fl}$ mice. F. Grassi, C.E. Faliti, E. Rottoli, and L. Perruzza analyzed data. G. Pellegrini performed histopathological analysis. M. Gerosa and R. Gualtierotti selected and provided human samples. R.L. Rossi performed PCA. E.M.C. Mazza and S. Bicciato performed meta-analysis of gene expression. C.E. Faliti, E. Rottoli, L. Perruzza, and F. Grassi prepared the figures. F. Grassi and C.E. Faliti wrote the paper. F. Grassi supervised the study.

Submitted: 1 November 2017
Revised: 22 October 2018
Accepted: 3 January 2019

References

Andreoli, L., C.B. Chighizola, C. Nalli, M. Gerosa, M.O. Borghi, F. Pregnolato, C. Grossi, A. Zanola, F. Allegri, G.L. Norman, et al. 2015. Clinical characterization of antiphospholipid syndrome by detection of IgG antibodies against β2 -glycoprotein i domain 1 and domain 4/5: ratio of anti-domain 1 to anti-domain 4/5 as a useful new biomarker for antiphospholipid syndrome. *Arthritis Rheumatol.* 67:2196–2204. https://doi.org/10.1002/art.39187

Arbuckle, M.R., M.T. McClain, M.V. Rubertone, R.H. Scofield, G.J. Dennis, J.A. James, and J.B. Harley. 2003. Development of autoantibodies before the clinical onset of systemic lupus erythematosus. *N. Engl. J. Med.* 349:1526–1533. https://doi.org/10.1056/NEJMoa021933

Blanco, P., H. Ueno, and N. Schmitt. 2016. T follicular helper (Tfh) cells in lupus: Activation and involvement in SLE pathogenesis. *Eur. J. Immunol.* 46:281–290. https://doi.org/10.1002/eji.201545760

Chen, G.M., C.C. Feng, Q.L. Ye, J.H. Tao, R. Li, H. Peng, M. Zhou, R.X. Leng, J. Li, H. Cen, et al. 2013. Association of P2X7R gene polymorphisms with systemic lupus erythematosus in a Chinese population. *Mutagenesis.* 28:351–355. https://doi.org/10.1093/mutage/get007

Choi, J.Y., J.H. Ho, S.G. Pasoto, V. Bunin, S.T. Kim, S. Carrasco, E.F. Borba, C.R. Gonçalves, P.R. Costa, E.G. Kallas, et al. 2015. Circulating follicular helper-like T cells in systemic lupus erythematosus: association with disease activity. *Arthritis Rheumatol.* 67:988–999. https://doi.org/10.1002/art.39020

Choi, Y.S., R. Kageyama, D. Eto, T.C. Escobar, R.J. Johnston, L. Monticelli, C. Lao, and S. Crotty. 2011. ICOS receptor instructs T follicular helper cell versus effector cell differentiation via induction of the transcriptional repressor Bcl6. *Immunity.* 34:932–946. https://doi.org/10.1016/j.immuni.2011.03.023

Chung, Y., S. Tanaka, F. Chu, R.I. Nurieva, G.J. Martinez, S. Rawal, Y.H. Wang, H. Lim, J.M. Reynolds, X.H. Zhou, et al. 2011. Follicular regulatory T cells expressing Foxp3 and Bcl-6 suppress germinal center reactions. *Nat. Med.* 17:983–988. https://doi.org/10.1038/nm.2426

Cohen, R.A., G. Bayliss, J.C. Crispin, G.F. Kane-Wanger, C.A. Van Beek, V.C. Kyttaris, I. Avalos, C.Y. Yu, G.C. Tsokos, and I.E. Stillman. 2008. T cells and in situ cryoglobulin deposition in the pathogenesis of lupus nephritis. *Clin. Immunol.* 128:1–7. https://doi.org/10.1016/j.clim.2008.04.004

Craft, J.E. 2012. Follicular helper T cells in immunity and systemic autoimmunity. *Nat. Rev. Rheumatol.* 8:337–347. https://doi.org/10.1038/nrrheum.2012.58

Crotty, S. 2014. T follicular helper cell differentiation, function, and roles in disease. *Immunity.* 41:529–542. https://doi.org/10.1016/j.immuni.2014.10.004

Ding, Y., J. Li, Q. Wu, P. Yang, B. Luo, S. Xie, K.M. Druey, A.J. Zajac, H.C. Hsu, and J.D. Mountz. 2013. IL-17RA is essential for optimal localization of follicular Th cells in the germinal center light zone to promote autoantibody-producing B cells. *J. Immunol.* 191:1614–1624. https://doi.org/10.4049/jimmunol.1300479

Domeier, P.P., S.B. Chodisetti, C. Soni, S.L. Schell, M.J. Elias, E.B. Wong, T.K. Cooper, D. Kitamura, and Z.S. Rahman. 2016. IFN-γ receptor and STAT1 signaling in B cells are central to spontaneous germinal center formation and autoimmunity. *J. Exp. Med.* 213:715–732. https://doi.org/10.1084/jem.20151722

Ferrari, D., C. Pizzirani, E. Adinolfi, R.M. Lemoli, A. Curti, M. Idzko, E. Panther, and F. Di Virgilio. 2006. The P2X7 receptor: a key player in IL-1 processing and release. *J. Immunol.* 176:3877–3883. https://doi.org/10.4049/jimmunol.176.7.3877

Geginat, J., F. Sallusto, and A. Lanzavecchia. 2001. Cytokine-driven proliferation and differentiation of human naive, central memory, and effector memory CD4(+) T cells. *J. Exp. Med.* 194:1711–1719. https://doi.org/10.1084/jem.194.12.1711

Gladman, D.D., D. Ibañez, and M.B. Urowitz. 2002. Systemic lupus erythematosus disease activity index 2000. *J. Rheumatol.* 29:288–291.

Hatzi, K., J.P. Nance, M.A. Kroenke, M. Bothwell, E.K. Haddad, A. Melnick, and S. Crotty. 2015. BCL6 orchestrates Tfh cell differentiation via multiple distinct mechanisms. *J. Exp. Med.* 212:539–553. https://doi.org/10.1084/jem.20141380

Havenar-Daughton, C., M. Lindqvist, A. Heit, J.E. Wu, S.M. Reiss, K. Kendric, S. Bélanger, S.P. Kasturi, E. Landais, R.S. Akondy, et al. IAVI Protocol C Principal Investigators. 2016. CXCL13 is a plasma biomarker of germinal center activity. *Proc. Natl. Acad. Sci. USA.* 113:2702–2707. https://doi.org/10.1073/pnas.1520112113

He, J., L.M. Tsai, Y.A. Leong, X. Hu, C.S. Ma, N. Chevalier, X. Sun, K. Vandenberg, S. Rockman, Y. Ding, et al. 2013. Circulating precursor CCR7(lo)PD-1(hi) CXCR5$^+$ CD4$^+$ T cells indicate Tfh cell activity and promote antibody responses upon antigen reexposure. *Immunity.* 39:770–781. https://doi.org/10.1016/j.immuni.2013.09.007

Hochberg, M.C. 1997. Updating the American College of Rheumatology revised criteria for the classification of systemic lupus erythematosus. *Arthritis Rheum.* 40:1725. https://doi.org/10.1002/art.1780400928

Huang, W., Q. Qi, J. Hu, F. Huang, T.M. Laufer, and A. August. 2014. Dendritic cell-MHC class II and Itk regulate functional development of regulatory innate memory CD4+ T cells in bone marrow transplantation. *J. Immunol.* 192:3435–3441. https://doi.org/10.4049/jimmunol.1303176

Hutloff, A., K. Büchner, K. Reiter, H.J. Baelde, M. Odendahl, A. Jacobi, T. Dörner, and R.A. Kroczek. 2004. Involvement of inducible costimulator in the exaggerated memory B cell and plasma cell generation in systemic lupus erythematosus. *Arthritis Rheum.* 50:3211–3220. https://doi.org/10.1002/art.20519

Ingegnoli, F., R. Gualtierotti, T. Schioppo, A. Orenti, P. Boracchi, C. Lubatti, C. Mastaglio, V. Galbiati, A. Murgo, S. Zeni, et al. 2014. Fibrosis biomarkers in isolated Raynaud's phenomenon: too little, too soon? *Ann. Rheum. Dis.* 73:940–941. https://doi.org/10.1136/annrheumdis-2013-204009

Irizarry, R.A., B. Hobbs, F. Collin, Y.D. Beazer-Barclay, K.J. Antonellis, U. Scherf, and T.P. Speed. 2003. Exploration, normalization, and summaries of high density oligonucleotide array probe level data. *Biostatistics.* 4:249–264. https://doi.org/10.1093/biostatistics/4.2.249

Jackson, S.W., H.M. Jacobs, T. Arkatkar, E.M. Dam, N.E. Scharping, N.S. Kolhatkar, B. Hou, J.H. Buckner, and D.J. Rawlings. 2016. B cell IFN-γ receptor signaling promotes autoimmune germinal centers via cell-intrinsic induction of BCL-6. *J. Exp. Med.* 213:733–750. https://doi.org/10.1084/jem.20151724

Kayagaki, N., I.B. Stowe, B.L. Lee, K. O'Rourke, K. Anderson, S. Warming, T. Cuellar, B. Haley, M. Roose-Girma, Q.T. Phung, et al. 2015. Caspase-11 cleaves gasdermin D for non-canonical inflammasome signalling. *Nature.* 526:666–671. https://doi.org/10.1038/nature15541

Khadra, A., M. Tomić, Z. Yan, H. Zemkova, A. Sherman, and S.S. Stojilkovic. 2013. Dual gating mechanism and function of P2X7 receptor channels. *Biophys. J.* 104:2612–2621. https://doi.org/10.1016/j.bpj.2013.05.006

Kim, Y.U., H. Lim, H.E. Jung, R.A. Wetsel, and Y. Chung. 2015. Regulation of autoimmune germinal center reactions in lupus-prone BXD2 mice by follicular helper T cells. *PLoS One.* 10:e0120294. https://doi.org/10.1371/journal.pone.0120294

Kitano, M., S. Moriyama, Y. Ando, M. Hikida, Y. Mori, T. Kurosaki, and T. Okada. 2011. Bcl6 protein expression shapes pre-germinal center B cell dynamics and follicular helper T cell heterogeneity. *Immunity.* 34:961–972. https://doi.org/10.1016/j.immuni.2011.03.025

Le Coz, C., A. Joublin, J.L. Pasquali, A.S. Korganow, H. Dumortier, and F. Monneaux. 2013. Circulating TFH subset distribution is strongly affected in lupus patients with an active disease. *PLoS One.* 8:e75319. https://doi.org/10.1371/journal.pone.0075319

Lee, S.K., D.G. Silva, J.L. Martin, A. Pratama, X. Hu, P.P. Chang, G. Walters, and C.G. Vinuesa. 2012. Interferon-γ excess leads to pathogenic accumulation of follicular helper T cells and germinal centers. *Immunity.* 37:880–892. https://doi.org/10.1016/j.immuni.2012.10.010

Le Gall, S.M., J. Legrand, M. Benbijja, H. Safya, K. Benihoud, J.M. Kanellopoulos, and P. Bobé. 2012. Loss of P2X7 receptor plasma membrane expression and function in pathogenic B220+ double-negative T lymphocytes of autoimmune MRL/lpr mice. *PLoS One.* 7:e52161. https://doi.org/10.1371/journal.pone.0052161

Linterman, M.A., W. Pierson, S.K. Lee, A. Kallies, S. Kawamoto, T.F. Rayner, M. Srivastava, D.P. Divekar, L. Beaton, J.J. Hogan, et al. 2011. Foxp3+ follicular regulatory T cells control the germinal center response. *Nat. Med.* 17:975–982. https://doi.org/10.1038/nm.2425

Locci, M., J.E. Wu, F. Arumemi, Z. Mikulski, C. Dahlberg, A.T. Miller, and S. Crotty. 2016. Activin A programs the differentiation of human TFH cells. *Nat. Immunol.* 17:976–984. https://doi.org/10.1038/ni.3494

McGuire, H.M., A. Vogelzang, C.S. Ma, W.E. Hughes, P.A. Silveira, S.G. Tangye, D. Christ, D. Fulcher, M. Falcone, and C. King. 2011. A subset of interleukin-21+ chemokine receptor CCR9+ T helper cells target accessory organs of the digestive system in autoimmunity. *Immunity.* 34:602–615. https://doi.org/10.1016/j.immuni.2011.01.021

Miyakis, S., M.D. Lockshin, T. Atsumi, D.W. Branch, R.L. Brey, R. Cervera, R.H. Derksen, P.G. DE Groot, T. Koike, P.L. Meroni, et al. 2006. International consensus statement on an update of the classification criteria for definite antiphospholipid syndrome (APS). *J. Thromb. Haemost.* 4:295–306. https://doi.org/10.1111/j.1538-7836.2006.01753.x

Moriyama, S., N. Takahashi, J.A. Green, S. Hori, M. Kubo, J.G. Cyster, and T. Okada. 2014. Sphingosine-1-phosphate receptor 2 is critical for follicular helper T cell retention in germinal centers. *J. Exp. Med.* 211:1297–1305. https://doi.org/10.1084/jem.20131666

Nacionales, D.C., J.S. Weinstein, X.J. Yan, E. Albesiano, P.Y. Lee, K.M. Kelly-Scumpia, R. Lyons, M. Satoh, N. Chiorazzi, and W.H. Reeves. 2009. B cell proliferation, somatic hypermutation, class switch recombination, and autoantibody production in ectopic lymphoid tissue in murine lupus. *J. Immunol.* 182:4226–4236. https://doi.org/10.4049/jimmunol.0800771

Nath, S.K., A.I. Quintero-Del-Rio, J. Kilpatrick, L. Feo, M. Ballesteros, and J.B. Harley. 2004. Linkage at 12q24 with systemic lupus erythematosus (SLE) is established and confirmed in Hispanic and European American families. *Am. J. Hum. Genet.* 74:73–82. https://doi.org/10.1086/380913

Nurieva, R.I., Y. Chung, D. Hwang, X.O. Yang, H.S. Kang, L. Ma, Y.H. Wang, S.S. Watowich, A.M. Jetten, Q. Tian, and C. Dong. 2008. Generation of T follicular helper cells is mediated by interleukin-21 but independent of T helper 1, 2, or 17 cell lineages. *Immunity.* 29:138–149. https://doi.org/10.1016/j.immuni.2008.05.009

Odegard, J.M., B.R. Marks, L.D. DiPlacido, A.C. Poholek, D.H. Kono, C. Dong, R.A. Flavell, and J. Craft. 2008. ICOS-dependent extrafollicular helper T cells elicit IgG production via IL-21 in systemic autoimmunity. *J. Exp. Med.* 205:2873–2886. https://doi.org/10.1084/jem.20080840

Odegard, J.M., L.D. DiPlacido, L. Greenwald, M. Kashgarian, D.H. Kono, C. Dong, R.A. Flavell, and J. Craft. 2009. ICOS controls effector function but not trafficking receptor expression of kidney-infiltrating effector T cells in murine lupus. *J. Immunol.* 182:4076–4084. https://doi.org/10.4049/jimmunol.0800758

Ohl, K., and K. Tenbrock. 2015. Regulatory T cells in systemic lupus erythematosus. *Eur. J. Immunol.* 45:344–355. https://doi.org/10.1002/eji.201344280

Pepper, M., A.J. Pagán, B.Z. Igyártó, J.J. Taylor, and M.K. Jenkins. 2011. Opposing signals from the Bcl6 transcription factor and the interleukin-2 receptor generate T helper 1 central and effector memory cells. *Immunity.* 35:583–595. https://doi.org/10.1016/j.immuni.2011.09.009

Poholek, A.C., K. Hansen, S.G. Hernandez, D. Eto, A. Chandele, J.S. Weinstein, X. Dong, J.M. Odegard, S.M. Kaech, A.L. Dent, et al. 2010. In vivo regulation of Bcl6 and T follicular helper cell development. *J. Immunol.* 185:313–326. https://doi.org/10.4049/jimmunol.0904023

Portales-Cervantes, L., P. Niño-Moreno, L. Doníz-Padilla, L. Baranda-Candido, M. García-Hernández, M. Salgado-Bustamante, R. González-Amaro, and D. Portales-Pérez. 2010. Expression and function of the P2X(7) purinergic receptor in patients with systemic lupus erythematosus and rheumatoid arthritis. *Hum. Immunol.* 71:818–825. https://doi.org/10.1016/j.humimm.2010.05.008

Proietti, M., V. Cornacchione, T. Rezzonico Jost, A. Romagnani, C.E. Faliti, L. Perruzza, R. Rigoni, E. Radaelli, F. Caprioli, S. Preziuso, et al. 2014. ATP-gated ionotropic P2X7 receptor controls follicular T helper cell numbers in Peyer's patches to promote host-microbiota mutualism. *Immunity.* 41:789–801. https://doi.org/10.1016/j.immuni.2014.10.010

Reeves, W.H., P.Y. Lee, J.S. Weinstein, M. Satoh, and L. Lu. 2009. Induction of autoimmunity by pristane and other naturally occurring hydrocarbons. *Trends Immunol.* 30:455–464. https://doi.org/10.1016/j.it.2009.06.003

Ruiz-Irastorza, G., M. Crowther, W. Branch, and M.A. Khamashta. 2010. Antiphospholipid syndrome. *Lancet.* 376:1498–1509. https://doi.org/10.1016/S0140-6736(10)60709-X

Satoh, M., and W.H. Reeves. 1994. Induction of lupus-associated autoantibodies in BALB/c mice by intraperitoneal injection of pristane. *J. Exp. Med.* 180:2341–2346. https://doi.org/10.1084/jem.180.6.2341

Schenk, U., M. Frascoli, M. Proietti, R. Geffers, E. Traggiai, J. Buer, C. Ricordi, A.M. Westendorf, and F. Grassi. 2011. ATP inhibits the generation and function of regulatory T cells through the activation of purinergic P2X receptors. *Sci. Signal.* 4:ra12. https://doi.org/10.1126/scisignal.2001270

Schindelin, J., I. Arganda-Carreras, E. Frise, V. Kaynig, M. Longair, T. Pietzsch, S. Preibisch, C. Rueden, S. Saalfeld, B. Schmid, et al. 2012. Fiji: an open-source platform for biological-image analysis. *Nat. Methods.* 9:676–682. https://doi.org/10.1038/nmeth.2019

Shi, J., Y. Zhao, K. Wang, X. Shi, Y. Wang, H. Huang, Y. Zhuang, T. Cai, F. Wang, and F. Shao. 2015. Cleavage of GSDMD by inflammatory caspases determines pyroptotic cell death. *Nature.* 526:660–665. https://doi.org/10.1038/nature15514

Skarnes, W.C., B. Rosen, A.P. West, M. Koutsourakis, W. Bushell, V. Iyer, A.O. Mujica, M. Thomas, J. Harrow, T. Cox, et al. 2011. A conditional knockout resource for the genome-wide study of mouse gene function. *Nature.* 474:337–342. https://doi.org/10.1038/nature10163

Stokes, L., S.J. Fuller, R. Sluyter, K.K. Skarratt, B.J. Gu, and J.S. Wiley. 2010. Two haplotypes of the P2X(7) receptor containing the Ala-348 to Thr polymorphism exhibit a gain-of-function effect and enhanced interleukin-1beta secretion. *FASEB J.* 24:2916–2927. https://doi.org/10.1096/fj.09-150862

Taylor, S.R., M. Gonzalez-Begne, S. Dewhurst, G. Chimini, C.F. Higgins, J.E. Melvin, and J.I. Elliott. 2008. Sequential shrinkage and swelling underlie P2X7-stimulated lymphocyte phosphatidylserine exposure and death. *J. Immunol.* 180:300–308. https://doi.org/10.4049/jimmunol.180.1.300

Teichmann, L.L., J.L. Cullen, M. Kashgarian, C. Dong, J. Craft, and M.J. Shlomchik. 2015. Local triggering of the ICOS coreceptor by CD11c(+) myeloid cells drives organ inflammation in lupus. *Immunity.* 42:552–565. https://doi.org/10.1016/j.immuni.2015.02.015

Ueno, H., J. Banchereau, and C.G. Vinuesa. 2015. Pathophysiology of T follicular helper cells in humans and mice. *Nat. Immunol.* 16:142–152. https://doi.org/10.1038/ni.3054

Vinuesa, C.G., M.C. Cook, C. Angelucci, V. Athanasopoulos, L. Rui, K.M. Hill, D. Yu, H. Domaschenz, B. Whittle, T. Lambe, et al. 2005. A RING-type ubiquitin ligase family member required to repress follicular helper T cells and autoimmunity. *Nature.* 435:452–458. https://doi.org/10.1038/nature03555

Vono, M., M. Taccone, P. Caccin, M. Gallotta, G. Donvito, S. Falzoni, E. Palmieri, M. Pallaoro, R. Rappuoli, F. Di Virgilio, et al. 2013. The adjuvant MF59 induces ATP release from muscle that potentiates response to vaccination. *Proc. Natl. Acad. Sci. USA.* 110:21095–21100. https://doi.org/10.1073/pnas.1319784110

Wang, B., Y. Yamamoto, N.S. El-Badri, and R.A. Good. 1999. Effective treatment of autoimmune disease and progressive renal disease by mixed bone-marrow transplantation that establishes a stable mixed chimerism in BXSB recipient mice. *Proc. Natl. Acad. Sci. USA.* 96:3012–3016. https://doi.org/10.1073/pnas.96.6.3012

Weber, J.P., F. Fuhrmann, R.K. Feist, A. Lahmann, M.S. Al Baz, L.J. Gentz, D. Vu Van, H.W. Mages, C. Haftmann, R. Riedel, et al. 2015. ICOS maintains the T follicular helper cell phenotype by down-regulating Krüppel-like factor 2. *J. Exp. Med.* 212:217–233. https://doi.org/10.1084/jem.20141432

Weinstein, J.S., M.J. Delano, Y. Xu, K.M. Kelly-Scumpia, D.C. Nacionales, Y. Li, P.Y. Lee, P.O. Scumpia, L. Yang, E. Sobel, et al. 2013. Maintenance of anti-Sm/RNP autoantibody production by plasma cells residing in ectopic lymphoid tissue and bone marrow memory B cells. *J. Immunol.* 190:3916–3927. https://doi.org/10.4049/jimmunol.1201880

Wilhelm, K., J. Ganesan, T. Müller, C. Dürr, M. Grimm, A. Beilhack, C.D. Krempl, S. Sorichter, U.V. Gerlach, E. Jüttner, et al. 2010. Graft-versus-host disease is enhanced by extracellular ATP activating P2X7R. *Nat. Med.* 16:1434–1438. https://doi.org/10.1038/nm.2242

Wollenberg, I., A. Agua-Doce, A. Hernández, C. Almeida, V.G. Oliveira, J. Faro, and L. Graca. 2011. Regulation of the germinal center reaction by Foxp3+ follicular regulatory T cells. *J. Immunol.* 187:4553–4560. https://doi.org/10.4049/jimmunol.1101328

Xu, H., X. Li, D. Liu, J. Li, X. Zhang, X. Chen, S. Hou, L. Peng, C. Xu, W. Liu, et al. 2013. Follicular T-helper cell recruitment governed by bystander B cells and ICOS-driven motility. *Nature.* 496:523–527. https://doi.org/10.1038/nature12058

Yang, X., J. Yang, Y. Chu, J. Wang, M. Guan, X. Zhu, Y. Xue, and H. Zou. 2013. T follicular helper cells mediate expansion of regulatory B cells via IL-21 in Lupus-prone MRL/lpr mice. *PLoS One.* 8:e62855. https://doi.org/10.1371/journal.pone.0062855

Yu, D., and C.G. Vinuesa. 2010. Multiple checkpoints keep follicular helper T cells under control to prevent autoimmunity. *Cell. Mol. Immunol.* 7:198–203. https://doi.org/10.1038/cmi.2010.18

Yusuf, I., R. Kageyama, L. Monticelli, R.J. Johnston, D. Ditoro, K. Hansen, B. Barnett, and S. Crotty. 2010. Germinal center T follicular helper cell IL-4 production is dependent on signaling lymphocytic activation molecule receptor (CD150). *J. Immunol.* 185:190–202. https://doi.org/10.4049/jimmunol.0903505

Zan, H., C. Tat, and P. Casali. 2014. MicroRNAs in lupus. *Autoimmunity.* 47:272–285. https://doi.org/10.3109/08916934.2014.915955